JGR Atmospheres

RESEARCH ARTICLE
10.1029/2022JD036518

Noah-MP With the Generic Crop Growth Model Gecros in the WRF Model: Effects of Dynamic Crop Growth on Land-Atmosphere Interaction

K. Warrach-Sagi[1], J. Ingwersen[2], T. Schwitalla[1], C. Troost[3], J. Aurbacher[4], L. Jach[1], T. Berger[3], T. Streck[2], and V. Wulfmeyer[1]

[1]Institute of Physics and Meteorology, University of Hohenheim, Stuttgart, Germany, [2]Institute of Soil Science and Land Evaluation, University of Hohenheim, Stuttgart, Germany, [3]Institute of Agricultural Sciences in the Tropics, University of Hohenheim, Stuttgart, Germany, [4]Institute of Farm and Agribusiness Management, Justus Liebig University Giessen, Giessen, Germany

Key Points:

- Coupling a crop growth model with the Weather and Research Forecasting model significantly improves the simulation of the leaf area index
- Land-atmosphere coupling strength is enhanced by weather dependent crop growth simulation
- The distributed added value metric shows a reduction in temperature biases of up to 80% in croplands throughout the season in Germany

Correspondence to:
K. Warrach-Sagi,
kirsten.warrach-sagi@uni-hohenheim.de

Citation:
Warrach-Sagi, K., Ingwersen, J., Schwitalla, T., Troost, C., Aurbacher, J., Jach, L., et al. (2022). Noah-MP with the generic crop growth model Gecros in the WRF model: Effects of dynamic crop growth on land-atmosphere interaction. *Journal of Geophysical Research: Atmospheres*, *127*, e2022JD036518. https://doi.org/10.1029/2022JD036518

Received 19 JAN 2022
Accepted 16 JUN 2022

Abstract In this paper we coupled a crop growth model to the Weather Research and Forecasting model with its land surface model Noah-MP and demonstrated the influence of the weather driven crop growth on land-atmosphere (L-A) feedback. An impact study was performed at the convection permitting scale of 3 km over Germany. While the leaf area index (LAI) in the control simulation was the same for all cropland grid cells, the inclusion of the crop growth model resulted in heterogeneous crop development with higher LAI and stronger seasonality. For the analyses of L-A coupling, a two-legged metric was applied based on soil moisture, latent heat flux and convective available potential energy. Weak atmospheric coupling is enhanced by the crop model, the terrestrial coupling determines the regions with the L-A feedback. The inclusion of the crop model turns regions with no L-A feedback on this path into regions with strong positive coupling. The number of non-atmospherically controlled days between April and August is increased by 10–15 days in more than 50% of Germany. Our work shows that this impact results in a reduction of both cold bias and warm biases and thus improves the metrics of distributed added value of the monthly mean temperatures. The study confirms that the simulation of the weather driven annual phenological development of croplands for the regional climate simulations in mid-latitudes is crucial due to the L-A feedback processes and the currently observed and expected future change in phenological phases.

1. Introduction

Croplands pose a special challenge to land surface modeling due to their large variety in properties in space and time that are related to differences in phenological development and crop management. Crop management includes cultivar selection, sowing and harvest dates, sowing density, and fertilization. Crop types like, winter and spring wheat, winter and spring barley, rapeseed, maize, soy beans, sugar beet or potatoes have different seasonal developments. Their crop-specific development stages significantly impact green leaf area index (LAI), green vegetation fraction (GVF), rooting depth, plant height, stomatal resistance, etc., and thus the energy flux partitioning at the land surface (Bohm et al., 2019; Gayler et al., 2014; Ingwersen et al., 2018; Wizemann et al., 2014). Crop growth models simulate the development stages of the crops including rooting depth, LAI and plant height in dependence of the weather, soil state, crop properties, and farmer crop management. Further, they simulate the actual stomatal resistance in dependence of the weather and plant dependent photosynthesis – all quantities impacting the transpiration and therefore land-atmosphere (L-A) feedback. In 2010, the Agricultural Model Intercomparison and Improvement Project was initiated to improve agricultural models based on their intercomparison and evaluation using high-quality global and regional data and best scientific practices (Asseng et al., 2013). Among the crop-models were Gecros (Yin & van Laar, 2005), Sucros (Goudriaan & van Laar, 1994) and Ceres (Ritchie et al., 1985) as part of the framework Expert-N (Biernath et al., 2011). These three crop-models are also available coupled to stand-alone land surface models of regional climate models (RCMs) (Ingwersen et al., 2018; van den Hoof et al., 2011; Zou et al., 2019).

Weather and climate in the mid-latitudes of the northern hemisphere widely depends on L-A interaction since the landscape is heterogeneous due to different soil properties and land cover as well as due to orography. Agricultural croplands show a weather dependent annual cycle of vegetation characteristics such as LAI, GVF and rooting depth. Santanello et al. (2018) give a detailed overview of the importance of L-A feedback in weather and

climate modeling and the history of L-A feedback modeling. Also, the Global Land-Atmosphere System Studies and LoCo (Local L-A Coupling) projects are introduced. This research resulted in a variety of metrics developed for studying L-A feedback quantitatively (Dirmeyer et al., 2012, 2014; Miralles et al., 2019; Vogel et al., 2018). This is especially important since the extremes like heavy precipitation events, droughts and heatwaves are expected to increase and show a strong dependence on L-A interaction (Zscheischler & Fischer, 2020). For instance, large-scale desert plantations have been proposed as a bio-geoengineering strategy to mitigate climate change by carbon sequestration and local climate modification (Becker et al., 2013; Wulfmeyer et al., 2014). Branch and Wulfmeyer (2019) developed a global feedback index to predict the impact of desert plantations on regional clouds and precipitation development. They "demonstrated that rainfall enhancement can be realized over desert agroforestry plantations and within a wide range of desert areas—a very exciting prospect for arid or semiarid regions." For Europe, Jach et al. (2020) applied LoCo metrics to RCM simulations from 1986 to 2015 in dependence of land-cover changes to regionalize the dominant L-A coupling pathways. They found, for example, that land use change modified the humidity and stability of the planetary boundary layer (PBL) by changing the surface flux partitioning.

Energy and water fluxes at the land surface and within the atmospheric boundary depend on the atmospheric, vegetation and soil state (Mahrt, 2000; Maronga & Raasch, 2013) that is, moisture, temperature and momentum in the PBL impacts and depends on the land surface. Milovac et al. (2016) showed that the surface energy fluxes in an RCM impact the temperature and moisture in the whole PBL as well as the entrainment fluxes at its top. Potential evapotranspiration is determined by LAI and rooting depth, that is, the plant; actual evapotranspiration is determined by the atmosphere. The interaction of exchange processes determines the water vapor pressure deficit of the leaves, the vegetation temperature, and the energy partitioning at the land surface. Since these depend both on the weather patterns and crop type, the current approach of frozen annual cycles of LAI and GVF of croplands in most RCMs results in errors in seasonal forecasts and climate simulations. Furthermore, crop growth and crop quality depend also on the atmospheric CO_2 concentration (Högy et al., 2019). The dependence of crop growth on atmospheric CO_2 concentration is included in sophisticated crop growth models and becomes important for climate projections. While the importance of crop models has already been addressed by global climate models (Osborne et al., 2007), their implementation in RCMs is a more sophisticated challenge and still in its infancy (Harding et al., 2015; Partridge et al., 2021). The reason is that with increasing grid resolution, dominant crop types emerge for each grid cell, which is relevant from a modeling perspective since for example, maize, soy beans, winter wheat and rapeseed show different weather and crop-dependent development. This means that in RCMs more specialized crop models need to be applied.

A shortcoming of almost all RCMs is the aforementioned static annual cycle of vegetation variables such as LAI and GVF in croplands. Most models applied in the Coordinated Downscaling Experiment (CORDEX) flagship pilot study on Land Use and Climate Across Scales do not apply dynamic vegetation simulation (Davin et al., 2019), neglecting that the annual cycle depends not only on the Julian day of the year and the vegetation class but are driven by the seasonal weather pattern. When they do apply a dynamic vegetation in croplands, they do not distinguish between different crops. Field experiments (Imukova et al., 2015; Ingwersen et al., 2011; Wizemann et al., 2014) show a strong year-to-year variation in the vegetation development in croplands in Germany and its dependence on the crop type. Further, high resolution satellite data (e.g., Copernicus Climate Change Service information, 2018) show the spatial and temporal year-to-year variability of the vegetation development. In particular, LAI is a crucial variable for the energy partitioning at the land surface resulting in a model sensitivity to L-A feedback (e.g., Mahowald et al., 2016; Williams & Torn, 2015).

State-of-the-art land surface models applied in RCMs use vegetation parameters set for vegetation types to calculate the energy and water fluxes at the surface, but most do not simulate the plant physiology and growth of leaves and roots. Croplands are only one category, neglecting that some crops (e.g., winter wheat) emerge already in late autumn and start growing in March while others like maize emerge in May (Ingwersen et al., 2018). Crop models applied in RCMs need to be coupled with their land surface models which exchange fluxes with the atmosphere every timestep, that is, within 5–60 s, depending on the spatial resolution. Further, they need to be parameterized for a wide range of crop varieties and be computationally efficient.

Ingwersen et al. (2018) described in detail the requirements for coupling a crop model originally developed for agricultural applications such as yield calculations to a land surface model of an atmospheric model. In their work, they exemplify this for the generic crop growth model Gecros (Yin & van Laar, 2005) and the land surface

model Noah-MP (Niu et al., 2011). Noah-MP as applied with the Weather Research and Forecasting model (WRF) (Skamarock et al., 2008) does not distinguish between the phenology development of crop types. Addressing this model limitat Ingwersen et al. (2018) and Liu et al. (2016) coupled crop models to the land surface model Noah-MP. Noah-MP-crop by Liu et al. (2016) was developed and parameterized for maize and soybean, two dominant crops in the central U.S. Ingwersen et al. (2018) coupled Gecros with Noah-MP to contrast the development of two major crops of mid Europe, maize and winter wheat, and analyzed the results at field sites in comparison with the standard Noah-MP cropland parameterization. Ingwersen et al. (2018) as well as Liu et al. (2016) demonstrated a better agreement of the magnitude and temporal development of the LAI by the simulations with the crop growth models. Liu et al. (2016) and Ingwersen et al. (2018) forced their simulations with observed weather data, that is, the results do not incorporate the L-A feedback. While Noah-MP-Gecros improved both latent and sensible heat fluxes, Noah-MP-Crop only improved the LAI and sensible heat flux, but not the latent heat flux. In contrast to Noah-MP-Crop, Noah-MP-Gecros includes dynamic root growth which is essential for root water uptake control and a dynamic harvest date. In these stand-alone simulations the simulated crop growth and resulting surface energy fluxes do not affect the atmospheric temperature, moisture and wind.

Partridge et al. (2021) conducted WRF-Noah-MP simulations coupled with the crop growth model of Noah-MP-crop for maize and soy beans in the USA. The crop model coupling improved the LAI but no significant change was found in in temperature and precipitation which they also attribute to the missing root growth dynamics and dynamic harvest dates. Root growth and harvest are both included in Gecros. Since crop growth is weather and crop-type dependent from sowing to harvest, the objective of this study is to analyze the impact of LAI simulated by a crop growth model on the L-A feedback. Following the coupling approach for Noah-MP-Gecros (Ingwersen et al., 2018), this study integrated Gecros into the source code of WRF-Noah-MP and investigates the impact on the L-A coupling strength for the 2005 growing season in Germany, in comparison to WRF-Noah-MP with its default table-based green LAI and rooting depth approach. Agricultural land covers 51% of the land surface in Germany (BMEL, 2017), of these 16,7 million ha about 70%,6% are cropland. Suitable metrics to quantify L-A feedback depend on the processes and the temporal, spatial and vertical scales of interest (Santanello et al., 2018) and available data source. One measure covering the daily to annual time scale and surface states, surface fluxes and the PBL is the two-legged coupling index (*TLCI*) with its atmospheric and terrestrial coupling indices (Dirmeyer, 2011; Guo et al., 2006; Santanello et al., 2018) and is therefore selected in this study to quantify the impact of a crop growth model on L-A feedback from April to August.

In the second section, the model setup, analysis metrics and case study are introduced. The impact of the crop model inclusion is shown in Section 3, the enhancement of the L-A coupling strength by the crop model is discussed in Section 4, and Section 5 concludes.

2. Materials and Methods

2.1. WRF Model Setup

This study applies the WRF model version 3.7.1 coupled with the land surface model Noah-MP on the convection permitting resolution of 0.03° (~3,057 m) and 50 vertical levels for Germany. The simulations were run on the CRAY XC40 at the High Performance Computing Center Stuttgart (HLRS) on 360 cores in Message Passing Interface mode. CMIP5 global climate simulations from 1960 to 2100 were downscaled with WRF within EURO- CORDEX (Warrach-Sagi et al., 2018) and ReKliEs-De (Hübener et al., 2017) to 0.11° (~12 km) resolution and have been made available in daily time intervals (https://esgf.llnl.gov/). Further ERA-Interim reanalysis data (Dee et al., 2011) from 1989 to 2009 was downscaled in this framework for evaluation. In this case study, the underlying 3-hourly (Tier2) data from July 2004 to August 2005 from this reanalysis driven WRF simulation was downscaled to 3 km. Within EURO-CORDEX, WRF is applied as a multi-physics ensemble by the participating institutions, that is, each institution applies a different set of parameterizations (Coppola et al., 2018; Davin et al., 2019; Jacob et al., 2020; Kotlarski et al., 2014). Building on the setup of the climate simulations of the University of Hohenheim within EURO-CORDEX (Bülow et al., 2019; Ivanov et al., 2018a, 2018b; Warrach-Sagi et al., 2013) in this study WRF was applied with the Morrison two-moment microphysics scheme (Morrison et al., 2009) and the radiation transfer models for long-wave and shortwave radiation CAM (Collins et al., 2004). Following the investigation of PBL schemes of WRF in Germany by Milovac et al. (2016) and the Arabian Peninsula by Schwitalla et al. (2020) the local MYNN-2 PBL scheme (Nakanishi & Niino, 2009) was selected. The land cover was based on the CORINE Land Cover (CLC) 2006 data, which was reclassified into the

IGBP-MODIS land cover types applied by WRF (Bauer et al., 2020). The applied soil texture data is based on the Harmonized World Soil Database (version 1.21) and available from Milovac et al. (2018).

2.2. Coupling Gecros With WRF-Noah-MP

The impact study of crop growth on L-A feedback requires the coupling of WRF with a land surface model which is able to simulate the phenological development of dominant crops in the region of interest. For this purpose, the crop model Gecros coupled with the land surface model Noah-MP and evaluated for croplands in Southwest Germany (Ingwersen et al., 2018) was implemented in WRF. The implementation of Gecros into WRF-Noah-MP is described in the following sections. Noah-MP multi-physics options were adopted from Ingwersen et al. (2018): table LAI and calculated GVF (opt_dveg = 3), soil moisture factor for stomatal resistance from Noah (opt_btr = 1), Topmodel-based runoff with groundwater (opt-run = 1), sensible heat exchange-coefficient based on Monin-Obukov-similarity theory (opt-sfc = 1), Koren's iteration for super-cooled liquid water (opt-frz = 1), two-stream radiation transfer scheme (opt-rad = 2), lower boundary of soil temperature in 8 m depth (opt-tbot = 2) and a semi-implisit snow/soil temperature time scheme (stc = 1). The LAI in the Noah-MP table is based on the global Moderate Resolution Imaging Spectroradiometer monthly climatology from 2000 to 2008 (Myneni et al., 2002; Yang et al., 2011).

The generic crop growth model Gecros, its coupling with Noah-MP, and its parameterization are described in detail in Ingwersen et al. (2018). In brief Gecros simulates, among others, the temporal evolution of leaf, stem, and root biomass. The phenological development of the crop is controlled by biological time, which depends on temperature. The partitioning of assimilates between root and shoot is simulated based on the functional balance theory (Yin & Schapendonk, 2004). The Gecros version implemented in Noah-MP was extended for vernalization, winter dormancy, germination and emergence routines. Gecros separates soil into a rooted and an unrooted zone. The rooted zone, the zone from which water is extracted by the crop, continuously expands until the maximum rooting depth is reached. Note that the rooting depth regulates the potential root water uptake of the plants and therefore impacts transpiration. To summarize, while Noah-MP applies a constant root depth of 1 m for cropland and a static annual cycle of the LAI, Noah-MP-Gecros simulates a dynamic above and below ground crop growth.

In Germany, winter wheat and maize are representatives of two contrasting crop groups. Imukova et al. (2015) termed "early-covering" crops, that is, crops that are sown in fall or early spring and already have a closed canopy in April/May (winter wheat, winter barley, winter rapeseed, winter oats, etc.) and "late-covering" crops, that is, crops that are sown in spring and have a closed canopy from June/July often well into September/October (maize, sugar beet, soybean). Noah-MP-Gecros was calibrated and validated on a comprehensive field data set of in total 16 site-years for winter wheat and maize. In the case of winter wheat, four phenological parameters and eight generic crop parameters were calibrated. The root mean square error of the LAI in the calibration and validation runs was 0.76 m^2/m^2 and 0.74 m^2/m^2, respectively. For the late-covering crop maize the obtained parameterization, however, showed a highly asymmetrical temperature sensitivity. By means of a sensitivity study, they demonstrated that a temperature bias of $\pm$1.5 K of a climate model directly propagates to the crop model which resulted in case of maize in poor crop simulations. An increase of 1.5 K moved the harvest day from 4 October to 30 August. A decrease by 1.5 K, in contrast, led to the situation that maize did not reach maturity. The temperature bias of RCMs is within this order of magnitude (Ivanov et al., 2018a; Kotlarski et al., 2014). Therefore, we applied Noah-MP-Gecros only for early-covering crops using the winter wheat parameterization, whose growth is not as sensitive to temperature bias as that of maize. For grid cells with cropland with dominant late-covering crops in Germany and outside of Germany, Noah-MP was applied without Gecros (see Section 2.3).

For the first time, we have implemented Gecros within an atmospheric model. Until the implementation into WRF version 3.7.1, introduced in this study, Gecros had only been coupled to the stand-alone version of Noah-MP and applied with a half-hourly time step (Ingwersen et al., 2018). This transition from the offline single-column model Noah-MP-Gecros to the parallelized code of the coupled WRF-Noah-MP-Gecros model required the inclusion of 60 prognostic spatially distributed variables related to the crops, their growth, ripening and harvest into WRF. Examples are development stage, leaf nitrogen, carbon in roots, stem and leaves and the distinction between green and total LAI. Gecros had to be adapted to simulate crop growth within every WRF-Noah-MP time step of a few seconds. Note that currently only early-covering crops are parameterized in WRF-Noah-MP-Gecros, other crops can be included in the future once the parameters are determined. Further, spatial maps for crop types simulated

by WRF-Noah-MP-Gecros and their sowing dates are required for each simulation year. WRF-Noah-MP calls the crop model for each cropland grid cell when it is identified as early-covering crop by the map. For all other grid cells the Gecros module is not called from Noah-MP, that is, in case of cropland grid cells the model currently distinguishes two crop types: Winter wheat, which is used for the representation of early-covering crops, and the default Noah-MP cropland parameters, which are used for representing all other crops. For all grid cells with default cropland, Noah-MP is called with the Ball-Berry photosynthesis scheme. For grid cells containing early-covering crops, land surface processes simulated with Noah-MP are thus extended by plant development and photosynthesis simulated with Gecros. Model simulation starts at the beginning of the cropping season before the first crops are sown, that is, after harvest in summer. Early-covering crops like winter wheat are sown in autumn and late-covering crops like maize are sown the following spring. Note that each grid cell is either early- or late covering crop because the model does not allow for a tile approach. To estimate the crop sowing dates, a cross-sectional analysis of observed sowing dates for winter wheat (doy_{seed}) in Germany was performed in dependence of a threshold date doy_{thr}, at which the remaining cumulated temperature sum (for the rest of the year) exceeds a given critical level based on the positive 2m-temperature difference to 5°C. The critical level of the remaining temperature sum is derived from observed sowing dates and was fixed for early-covering crops in this study to 170.62 K. It was derived from 31 pairs of climate and phenological observation stations spread in Germany which were less than 10 km apart, deviated in altitude by less than 100 m. Only observations that provided at least 10 observations ending after 2010 were included in the regression. Years were treated as fixed effects. The empirical regression obtained (F statistics: 15.43; standard error (doy_{thr}): 0.04196; t value (doy_{thr}): 6.258) was

$$doy_{seed} = 206.84 + 0.26255\, doy_{thr} \quad (1)$$

Farmer crop management other than sowing and harvest, for example, tillage, fertilization and plant protection was not explicitly modeled. Hence, we assume a healthy crop stand with nutrients well-supplied. Crop harvest in the model occurred at simulated crop maturity. Following their early-covering crops, farmers in Germany typically grow a catch crop (e.g., mustard or phacelia). To capture this crop rotation in our simulations, the LAI in grid cells after early harvest was set to 0.7 m^2/m^2. An LAI of 0.7 m^2/m^2 reflects the situation that the soil is usally not fully baer after harvest. After harvest the soil may be covered with an intermediate crop, volunteer cereals or weeds.

2.3. Case Study: Growing Season 2005 in Germany

2.3.1. Configuration of the Case Study

Germany is characterized by gradients in the phenological phases due to both maritime to continental climate from North to South, and altitudes changes between coastal lowlands in the North to the Alps in the South-east, with low mountain ranges in between. The Rhine valley in the West is characterized by a warm and mild climate and therefore an early start of the growing season. Two 1-year simulations were run for the case study: WRF-Noah-MP was applied as control simulation (CTRL) and WRF-Noah-MP-Gecros for the experiment (EXP_CROP) from July 2004 to August 2005. Simulation of early-covering crops with Gecros in EXP_CROP was confined to grid cells within Germany only, and grid cells outside Germany were simulated with as in CTRL, because (a) the winter wheat parameterization applied has so far only been evaluated for Germany (Ingwersen et al., 2018) and (b) fully covering phenological observations were available for Germany only. This means CTRL and EXP_CROP differ for cropland grid cells with early covering crops, where instead of applying prescribed values Gecros calculates the LAI, rooting depth and plant height. The analysis of the growing season requires the model simulation to start before the first sowing dates of the early-covering crops – meaning before September in Germany. For the case study, we deliberately selected a year without extreme events because a drought like 2003 will severly impact the surface energy balance regardless of the crop parameterization. Weather data from the German Weather Service (DWD, 2019) shows that with respect to the reference period 1981–2010, the period from summer 2004 to summer 2005 was a normal weather period in Germany, as the mean seasonal temperatures and precipitation did not deviate by more than 0.3 K and 5%. During this period no droughts occurred, that is, evapotranspiration was mainly modulated by soil moisture variation, vegetation properties, and weather. Figure 1 shows the orography, soil texture data and land cover types aggregated to the model resolution with the WRF

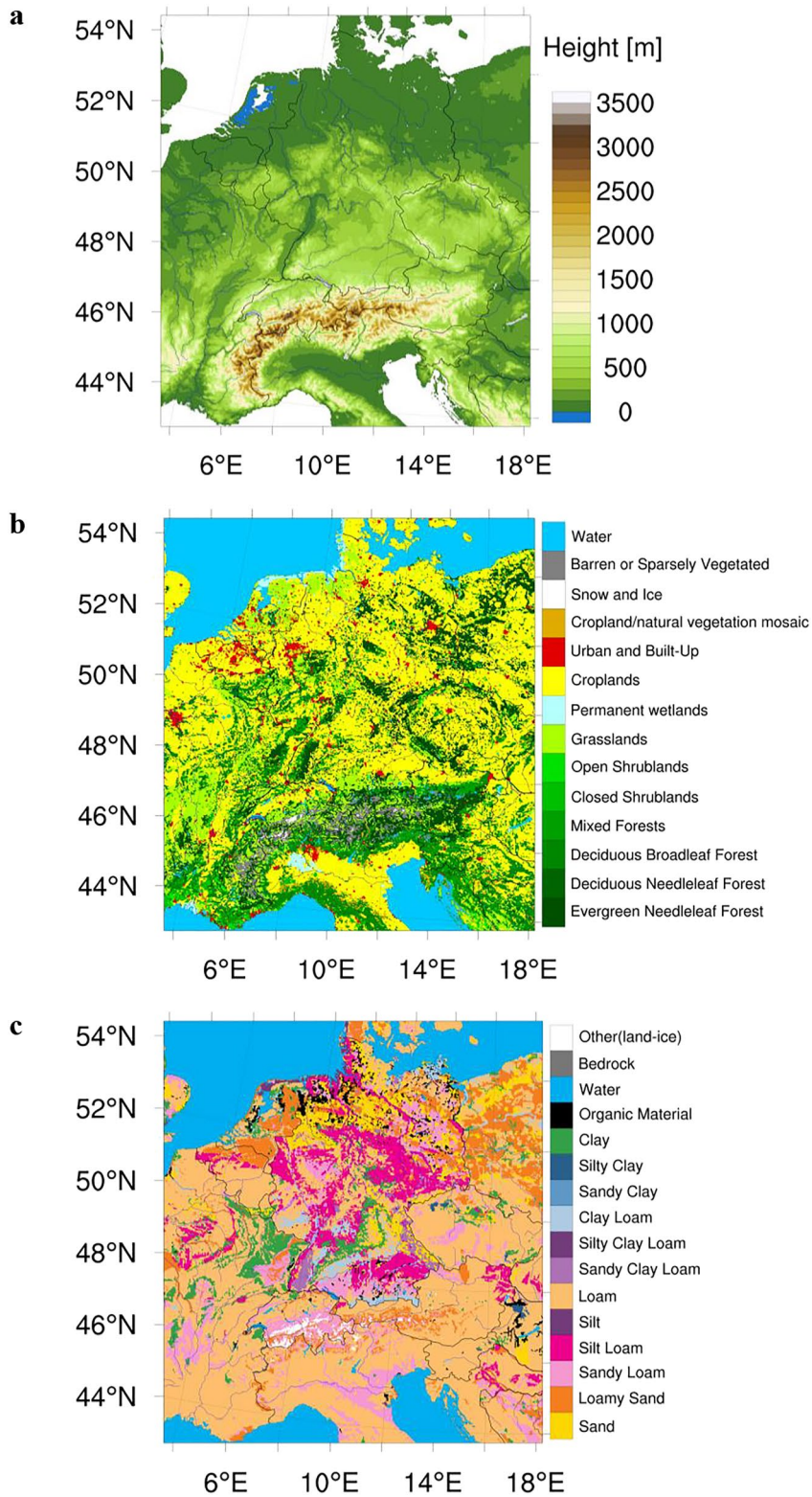

Figure 1. Static fields for Weather Research and Forecasting (WRF) in the model domain aggregated to the model grid resolution of 0.03° with the WRF pre-processing system. (a) Orography, (b) IGBP-MODIS vegetation classification of WRF based on CORINE Land Cover (CLC) 2006 data (Bauer et al., 2020) and (c) soil texture (based on Harmonized World Soil Database (version 1.21)) (Milovac et al., 2018).

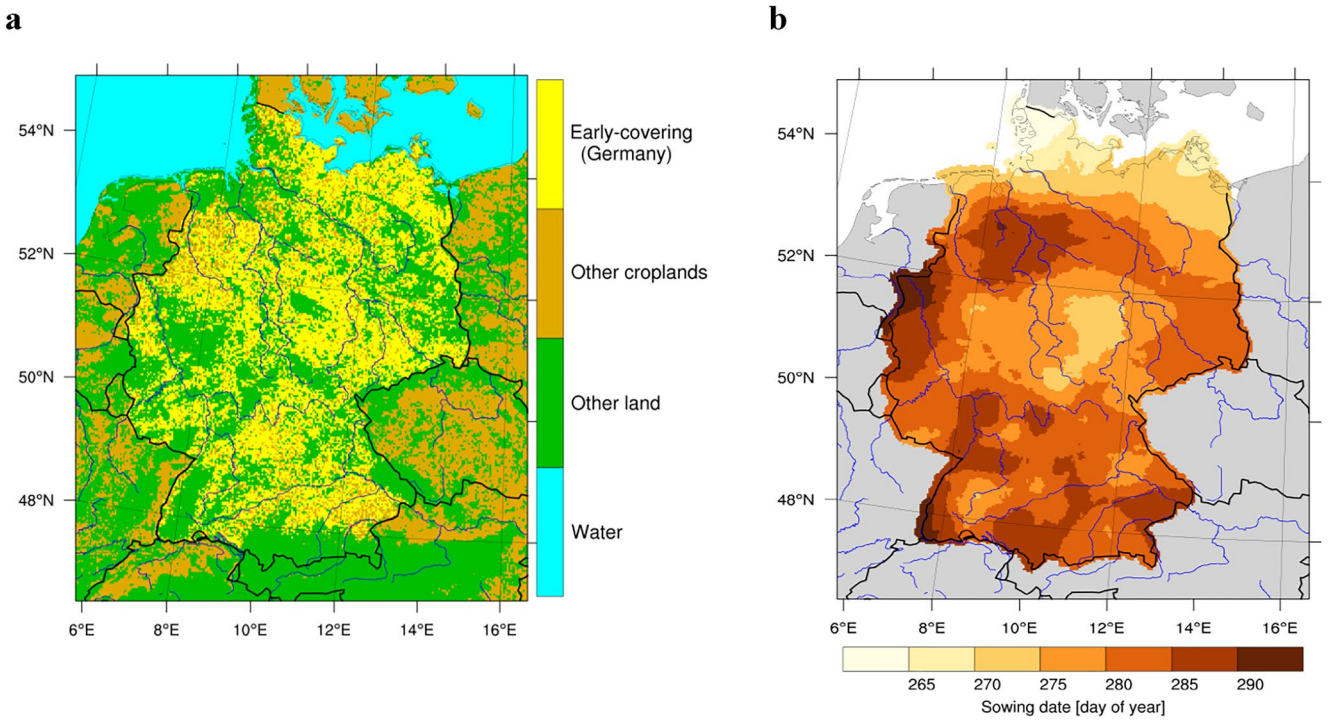

Figure 2. (a) Map for the application of Noah-MP-Gecros (early-covering crops) and Noah-MP (Other cropland and other land), (b) sowing date [julian day] for early-covering crops in Germany.

pre-processing system over the simulation domain of 392 × 436 grid cells. The WRF pre-processing aggregates the soil texture and land cover type based on the dominant class.

2.3.2. Crop Maps

For our case study, we needed to define those cropland cells where the Gecros winter wheat simulation was performed. We considered the winter wheat simulation as representative for early-covering crops (in Germany mainly: winter wheat, winter barley, spring barley, winter rapeseed, rye, oats and potatoes). The Noah-MP default parameterization is considered representative for late-covering crops (in Germany: maize, soybean or sugar beet). We used agricultural land use data from the 2010 Agricultural Census, which is publicly available at the district (NUTS3) level, to determine the share of late-covering crops (maize, soybean, sugar beet) in each German municipal district. By overlaying the district map and the vegetation type input map, we identified the WRF 0.03° grid cells with vegetation type cropland that belonged to each district and randomly categorized each cell as being covered by either late-covering crops or early-covering crops using the late-covering crop share as probability for the random allocation. In this way, the overall crop type share in each district could be preserved in the map, although this procedure led to a more agglomerated land use pattern than in reality, where different crops are more finely intermixed at typical plot sizes between 1 and 10 ha and alternating between cells from season to season due to crop rotation.

An alternative allocation approach was also tested, which first realized the random allocation at a grid resolution of 1 ha in order to then aggregate to the 0.03° WRF resolution by the largest area fraction principle. Due to the relative dominance of early-covering crops in nearly all areas, however, this second approach reduced the overall late-covering crop share in the input map to ∼2.5% of German cropland compared with ∼21% in reality. For this experiment, we decided that the error introduced by such a gross underrepresentation of the total area would likely be more distorting than the error introduced by the aforementioned overagglomeration of crop type areas, thus the first approach was kept.

Figure 2a shows the cropland grid cells and early-covering crop grid cells in the model domain. As mentioned above, sowing and harvesting dates were made dynamic in our WRF-Noah-MP-Gecros simulation study. For the sowing dates of winter wheat, the relationship found in formula 1 was applied to all grid cells, taking a weighted

average of six past years of the cumulated temperature sums into account. Figure 2b shows the sowing dates applied in this case study. Harvest was assumed in dependence of crop maturity as simulated by Gecros.

2.4. Data and Validation Metrics

2.4.1. Observational Data for Evaluation

Simulation results were evaluated for the main growing season of early – covering crops from April to August. The evolution of the LAI was compared with Copernicus Climate Change Service (C3S) satellite derived data (Copernicus Climate Change Service information, 2018) and the temperature (2 m height) with gridded observational data (OBS) from the German Weather Service (Krähenmann et al., 2016). The C3S LAI data set version 1.0 is available at 1 km horizontal resolution at a temporal resolution of 10 days for the study period from SPOT/VEGETATION. Camacho et al. (2013) evaluated the LAI data against ground data and found "very good agreement across the whole range of LAI values, with a slight underestimation for the highest values." Both, the C3S LAI data set and the temperature data set were regridded to the model grid applying the nearest neighbor method with the CDO (Climate Data Operators) software (Schulzweida, 2019).

2.4.2. Distribution Added Value

The distribution added value (*DAV*) developed by Soares et al. (2017) is a statistical metric based on the Perkins Skill Score (Perkins et al., 2007) to analyze statistically the overlap of the pdfs of a variable in order to study the added value of a higher model resolution. Here we apply this metric to analyze monthly mean temperatures of CTRL and EXP_CROP in comparison with OBS:

$$DAV = \frac{S_{EXP\_CROP} - S_{CTRL}}{S_{CTRL}} = \frac{\sum_1^n \min\left(Z_{EXP\_CROP}, Z_{OBS}\right) - \sum_1^n \min\left(Z_{CTRL}, Z_{OBS}\right)}{\sum_1^n \min\left(Z_{CTRL}, Z_{OBS}\right)} \quad (2)$$

S is the Perkins Skill Score, n is the number of bins of the pdf of the analyzed variable, Z is the frequency of values in a given bin. A positive *DAV* indicates a larger overlap of the area underneath the pdfs of Z_{EXP_CROP} with OBS than Z_{CTRL} and OBS, a negative value of *DAV* is a loss and 0 indicates no gain by EXP_CROP.

2.4.3. Land Atmosphere Coupling Strength Metrics

Santanello et al. (2018) gave an overview of statistical and process-based metrics suitable to quantify the L-A coupling. LoCo strength was analyzed using soil moisture η, latent heat flux *LH* and convective available potential energy (*CAPE*) because we were mainly interested whether the incorporation of crop growth had an influence on the likelihood of convection initiation. *LH* and soil moisture η are prognostic variables and *CAPE* is calculated from prognostic variables, while the PBL height depends on the parameters and threshold values of the diagnostics of the applied turbulence parameterization in WRF. For 2000–2008 from northern to southern Germany, Rüdisühli et al. (2020) identified ∼20%–∼50% summer precipitation as convective eventsunder weak synoptic conditions. *CAPE* is a measure for the atmospheric stability and depends on the atmospheric humidity which is related to the latent heat flux among others. Large values show the potential that subsequent convection may have. Note, that whether convection is ultimately triggered and whether this leads to convective precipitation depends on further atmospheric conditions that are not the subject of this study. For daily, monthly and annual timescale a statistic based LoCo metric to study the process chain between surface states, surface fluxes and PBL properties are the terrestrial coupling index (*TCI*), the atmospheric coupling index (*ACI*) and the *TLCI* developed by Guo et al. (2006) and Dirmeyer (2011). The coupling strength of TCI *TCI*, noting the relationship

$$TCI = \sigma(\eta)\frac{dLH}{d\eta} \quad (3)$$

where d*LH*/dη is the slope of the linear regression between *LH* and η, and $\sigma(\eta)$ stands for the standard deviation of η (Santanello et al., 2018). Further, the *ACI* between the daytime (6–21 UTC) *LH* and the maximum daily convective available potential energy (*CAPE*) can be calculated as:

$$ACI = \sigma(LH)\frac{dCAPE}{dLH} \quad (4)$$

For the *TLCI* the regression results in

$$TLCI = \sigma(\eta)\frac{dLH}{d\eta}\frac{dCAPE}{dLH} \quad (5)$$

All these coupling indices are based on a linear regression of considered variables and weighted by the standard deviation of the considered base line variable (Jach et al., 2020). The indices recognize that it is not sufficient to consider the correlation between two variables to quantify the coupling strength. There needs also to be sufficient variability over time in the base line variable. For a reliable regression a time series of at least 100 days is needed. Therefore, the coupling strength was calculated for April to August. Results were tested on the 97.5% significance level applying the Student-t test. Grid cells showing no significance are excluded from the analyses.

Following Jach et al. (2020) the analyses are complemented by a comparison of the frequency of non-atmospherically controlled (*nAC*) days from both simulations. *nAC* is based on the process metric convective triggering potential-low-level humidity index. Process-level metrics can be used as a diagnostic tool to represent L-A feedback in model simulations (https://www.pauldirmeyer.com/coupling-metrics) or from various data sources (Wakefield et al., 2021). *nAC* days have intermediate moisture levels and unstable conditions in the lower atmosphere around sunrise (Findell & Eltahir, 2003), which allow turbulent heat flux distribution to influence locally triggered deep convection during the following day. On the other hand, on atmospherically controlled days, atmospheric conditions probably prevent a decisive influence of the land surface on deep convection. First and foremost, differences in the frequency of *nAC* days indicate an influence of vegetation on the average ABL moisture and/or stability, which in turn suggests an L-A feedback on the seasonal time scale. Second, an increase in the frequency of *nAC* days indicates a higher relevance of the land surface for convective processes, which in turn indicates an L-A feedback on the diurnal time scale.

The three metrics *TCI*(η,*LH*), *ACI*(*LH, CAPE*) and *TCLI*(η, *LH,CAPE*) and *nAC* days were chosen to study if the inclusion of a crop growth model impacts the simulated L-A coupling strength and to which extent this is along the terrestrial leg, the atmospheric leg or the whole chain. The three coupling indices were calculated applying the portable FORTRAN 90 code modules from the open-source code package Coupling Metrics Toolkit (CoMeT, 2016; www.coupling-metrics.com) wrapped into a NCAR Common Language (NCL) code program.

3. Results

Compared to CTRL, the crop model in EXP_CROP changes the rooting depth and LAI. This changes soil moisture content, soil and vegetation temperature, and energy fluxes between the land surface and the atmosphere. The fluxes also depend on the atmospheric state (temperature, humidity, wind speed) and they also impact *CAPE*. Cold/warm temperatures in spring would cause a slow/fast crop growth and development of LAI and rooting depth. A low/high LAI and rooting depth allow less/more evapotranspiration when the soil moisture and energy is not limited. If the soil moisture limits the evapotranspiration, this impacts the sensible heat flux. The surface energy fluxes impact the atmospheric state and stability, *CAPE* can be used to express the differences in the impact in the simulations. EXP_CROP and CTRL differences in LAI, temperature and L-A feedback are connected, however, atmospheric advection and precipitation are a result and additional impact. In the following the results for LAI and temperature are evaluated and the resulting atmospheric coupling strengths EXP_CROP and CTRL are shown.

3.1. Crop Growth Simulation: The Leaf Area Index

The area of a single grid cell of the CTRL, EXP_CROP and C3S is 900 ha. A grid cell of this size classified as cropland in Germany is covered with several early and late covering crops and it is fragmented by hedges, forest patches, villages and roads. In CTRL the LAI of a cropland grid cell is not simulated but taken from a table. In EXP_CROP a grid cell with early-covering crops takes the LAI value of a single simulated crop (winter wheat). The satellite derived gridded data set C3S shows the effective LAI of a grid cell. that is, grid cells classified as cropland in CTRL and EXP_CROP (Figure 2a) in C3S have the dominant vegetation class cropland but also include the signals of other vegetation classes but also roads and buildings. For the gridded data C3S has a mean bias of -0.25 m^2/m^2, a RSME of 0.79 and a correlation of 0.87 in comparison with ground data (Fuster Ochando & Sánchez-Zapero, 2019). To allow a comparison between simulated and observed LAI only grid cells classified as early-covering crops (see Figure 2a) with more than 60% cropland are analyzed. These are colored grid cells

in Figure 3, which shows the LAI for five selected dates during the growth, ripening and harvest of agricultural crops from April to August for the CTRL and EXP_CROP simulations in comparison with the OBS set C3S. C3S (Figure 3, left column) shows a clear seasonal cycle with lowest values in spring, maximum LAI values of up to 6 m^2/m^2 at the end of June and declining values over the ripening and harvest period in July and August. Further, a pronounced spatial heterogeneity is visible in the maps with the fully developed LAI on 30 June and the following decline, which is more rapid in central Germany, because there the crops were fully developed earlier on, resulting in an earlier ripening and harvest.

In CTRL (Figure 3, right column), all crop grid cells show uniform values of LAI following a temporal cycle without any spatial heterogeneity. Note, CTRL does not distinguish between the green and total LAI. In particular, the CTRL simulation underestimates LAI values until the end of June. In July and August, instead of showing declining LAI values, as expected due the maturing of early-covering crops, the LAI values remain on the maximum level.

The EXP_CROP simulation (Figure 3, middle column) produces a distinct spatial heterogeneity in April and July due to weather dependent growth and ripening. Until 20 May the LAI developed in all grid cells, ripening (and resulting decline) occurs in July. On 20 August most early covering crops were harvested and a catch crop is assumed. In April EXP_CROP alike C3S shows an increase in LAI. In central Germany and along the Baltic sea it is larger than in C3S. Regions in central Germany showing an LAI above 2 m^2/m^2 on 10 April coincide with an early sowing date the previous autumn (see Figure 2b). Early-covering crops already emerge in autumn and then fall into dormancy until spring. So the crops in these grid cells already had more time to grow than in other areas. In EXP_CROP the sowing date is based on the climatological temperature (see Section 2.2). At the end of July and August, the ripening and harvest is visible in C3S indicated by lower LAIs. This ripening and harvest occurs delayed in EXP_CROP except for western Germany, where it occurs too early. But its distribution is well visible while CTRL still shows the maximum LAI and no spatial heterogeneity.

The temporal evolution of the spatially averaged LAI of grid cells with more than 60% cropland classified as early covering crops for four subdomains with different LAI cycles is shown in Figure 4. The subdomains were selected according to sowing date (Figure 2b) and geographical location. The location of the four subdomains - Central Germany (A), Western Pomerania in North-Eastern Germany (B), Rhine Valley in Western Germany (C) and Lower Bavaria in South-Eastern Germany (D) - are shown in Figure 4e. The C3S data show a pronounced seasonal cycle starting with an LAI of 1.1–1.5 m^2/m^2 in April. In Central and Western Germany (Fig. 4a, c), a LAI maximum of 5 m^2/m^2 and 3.5 m^2/m^2, respectively, is reached on 20 June. In July, due to maturity, harvest and catch crops, the LAI decreases to 1.7 m^2/m^2 and 1.9 m^2/m^2 respectively by 10 August. In North-Eastern and South-Eastern Germany (Figures 4b and 4d), the maximum LAI of 4.9 m^2/m^2 and 3.4 m^2/m^2, respectively, is reached on 30 June. In July and August, there was a rapid decline in LAI in North-Eastern Germany, while in South-Eastern Germany the decline was much slower and was still 2.2 m2/m2 at the end of August.

Due to the static annual cycle of cropland LAI in CTRL, this simulation produces a uniform seasonal cycle in all subdomains with maxima of 3 m^2/m^2 in August and crop emergency on the 15 April. In Central and North-Eastern Germany (Figures 4a and 4b) the simulated CTRL cycle is also delayed by 2 months and reached maxima on 10 August are 2 m^2/m^2 too low. In the Rhine Valley and South-Eastern Germany (Figures 4c and 4d) the CTRL maxima are 0.5 m^2/m^2 lower than the C3S maxima and delayed by 1 month. In contrast to CTRL, EXP_CROP simulates LAI in grid cells of early-covering crops, therefore the time series differ for each sub-domain as in C3S. For Central Germany (Figure 4a), EXP_CROP simulates an LAI maximum of 4.7 m^2/m^2, which is 0.3 m^2/m^2 lower and 1.5 months too early. In North-Eastern Germany (Figure 4b) the simulated LAI shows a similar behavior with a maximum LAI of 4.4 m^2/m^2 on 20 May. In the Rhine Valley (Figure 4c), EXP_CROP simulates the C3S LAI on 10 April and 20 August. It increases too much until 20 May, when the LAI is 4.0 m^2/m^2, while C3S has a LAI of 2.6 and CTRL 0.7 m^2/m^2. In South-Eastern Germany (Figure 4d) EXP_CROP slightly underestimates the observed increase in April by 0.3–0.8 m^2/m^2. Atmospheric temperature biases in the lowest atmospheric layer of the model carry over to the plant model and influence the pace of plant development. April shows a warm bias (see Section 4.2), which leads to an over-rapid plant growth.

Summarizing the comparison of CTRL and EXP_CROP with C3S in the four subdomains the CTRL simulation does not show the observed regional weather dependence of the growth and decline in LAI, that is, the maxima are underestimated especially in central and northern Germany and delayed by 1 month. Despite the plausible

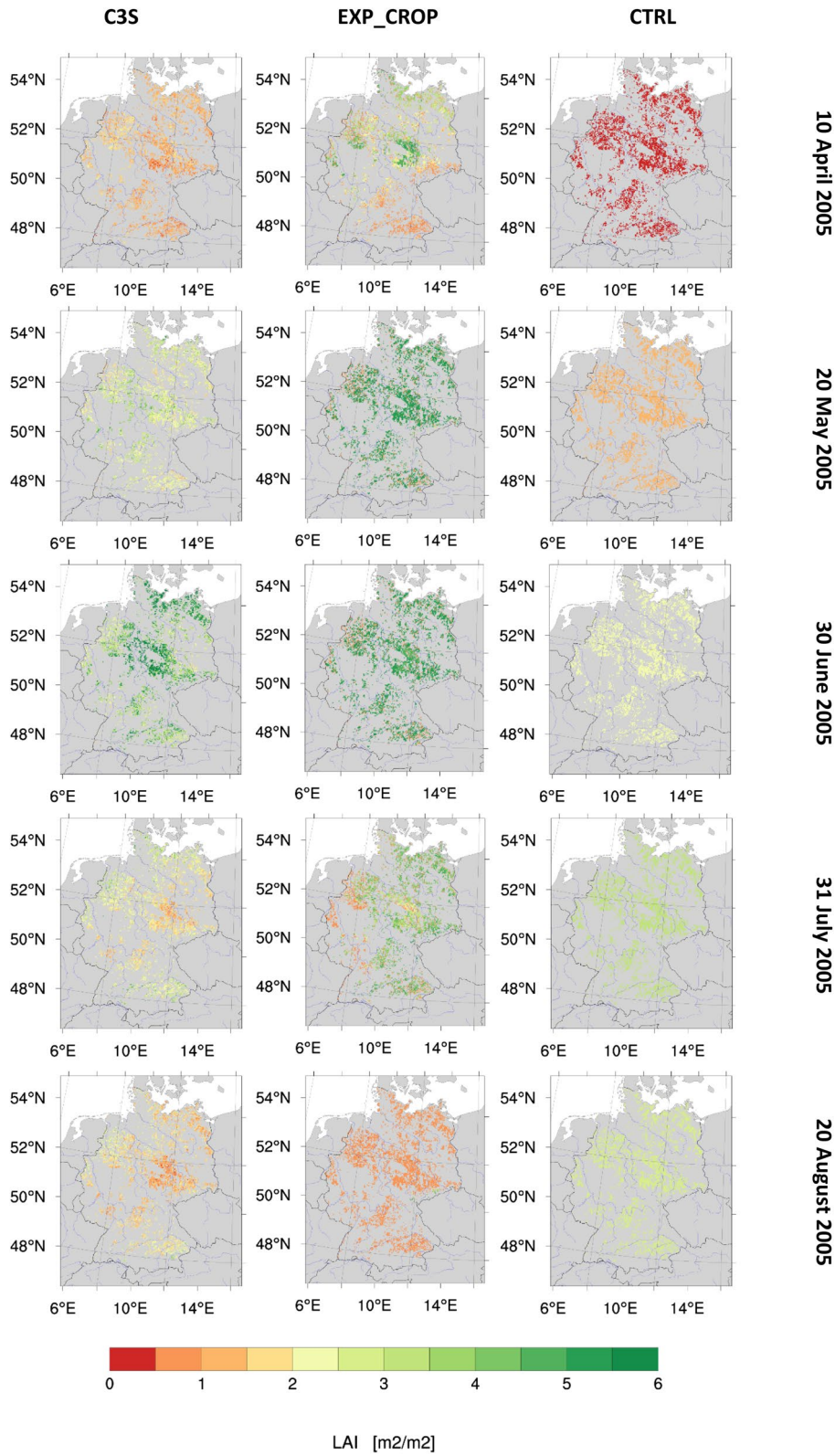

Figure 3. Green leaf area index (LAI) [m^2/m^2] from the satellite derived data Copernicus Climate Change Service (C3S), and the simulations EXP_CROP and control simulation (CTRL) for early-covering cropland gridcells with more than 60% cropland. Note, CTRL does not distinguish between the green and total LAI.

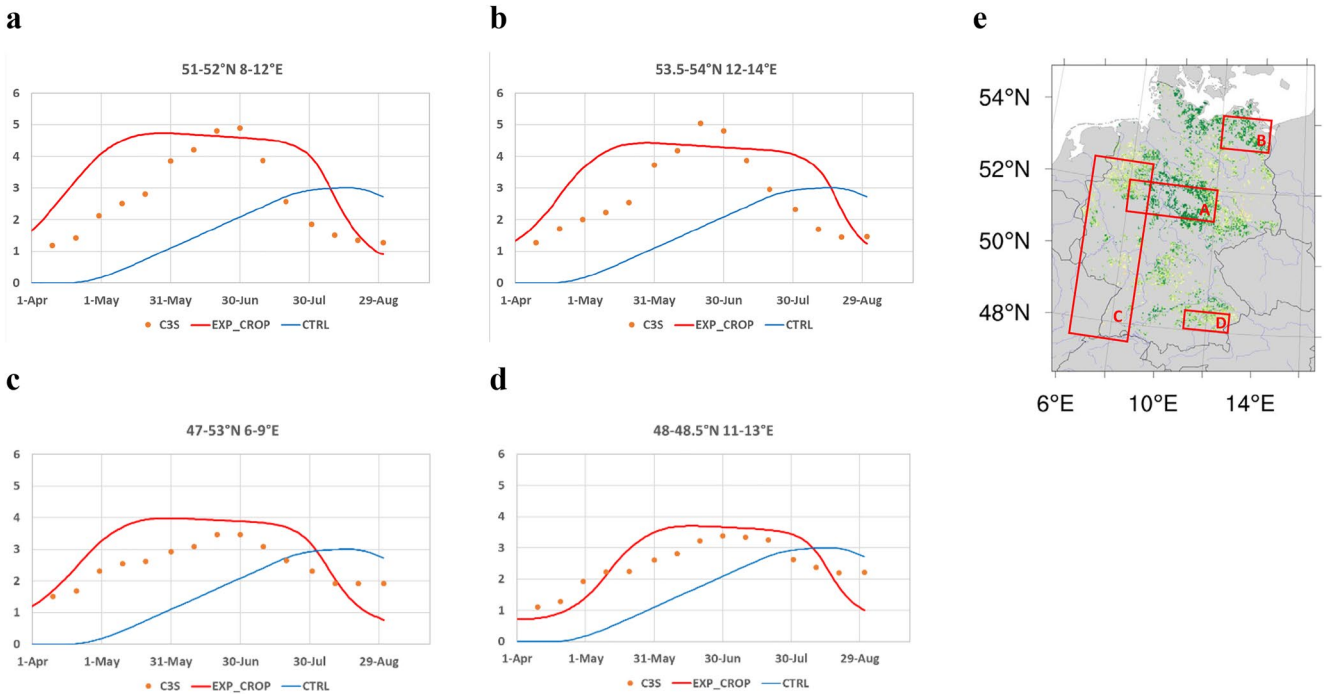

Figure 4. Areal mean green leaf area index (LAI) [m^2/m^2] from the satellite derived data Copernicus Climate Change Service (C3S), and the simulations EXP_CROP and control simulation (CTRL) for early-covering cropland gridcells with more than 60% cropland of selected subdomains: (a) Central Germany, (b) Western Pommerania in North East Germany, (c) Rhine Valley in West Germany, (d) Lower Bavaria in South East Germany. (e) shows the location of the subdomains A-D in the C3S LAI displayed in Figure 3 for the 30 June 2005. Note, CTRL does not distinguish between the green and total LAI.

overestimation of LAI between Mid-May and Mid-June during the growing period in EXP_CROP, its simulated spatial pattern and temporal variations shows the crop's growth condition in response to the weather, which has more agreement with C3S than CTRL.

From Figures 3 and 4, it can be seen that the crop growth model is essential to capture the weather and crop dependent spatial heterogeneity and temporal development of the LAI. This cannot be achieved by standard table values derived for given climate such as crops and sowing density. For two locations in Southwest Germany, Ingwersen et al. (2011, 2018) and Wizemann et al. (2014) demonstrated on the basis of multi-year field measurements that major crops (winter rapeseed, winter wheat, winter barley, silage maize) have a weather dependent temporal development. Depending on the year's and region's weather, differences between the LAI development of EXP_CROP and C3S were of a similar order. The maximum LAI level of the CTRL run was distinctly lower than in the EXP_CROP run. This lower LAI in the CTRL run and its shifted seasonal cycle reflects that Noah-MP was developed for the conditions of the US and represents their representative mix of crops. Note that in the US, crop production is less intensive than in Germany. Winter wheat is drilled with larger row-spacing, nitrogen fertilization rates are less than half of those applied by German farmers, and soils are usually neither plowed nor worked with a harrow/cultivator. Consequently, crop yields per hectare and also the LAI values are considerably lower than in Germany. While at the sites that were used for calibrating Gecros the average winter wheat yield was 8.3 t/ha between the years 2016–2018, in the same time frame the average winter wheat yield in the US was 3.4 t/ha (USDA, 2019). LAI values in the “breadbasket” of the US, the great plains, are rarely exceeding values of three (Y. Lu et al., 2017).

The comparison underlines the necessity of including more crop types and especially catch crops in the simulations to reach observed grid scale LAIs.

3.2. Temperature

Temperature is a variable of major interest in weather and climate research. It is also a key forcing variable for impact models. Since the temperature does not only depend on synoptic weather conditions but also on coupled L-A processes, differences in the temperature at 2-m height of CTRL and EXP_CROP simulations are analyzed.

Figure 5 shows the gridpoint time series of the mean monthly temperatures in Germany for April–August 2005 pooled together in probability density functions (PDFs for CTRL, EXP_CROP and OBS). The *DAV* (Equation 2) is calculated for each month and displayed in each figure. In April and May, higher temperatures than observed are simulated, while in June lower temperatures than observed are simulated. In July the pdfs of the simulated temperatures are too flat indicating an overestimation of the lower and higher temperature quantiles and an underestimation of the middle part. From April to July the *DAV* shows an added value of the implementation of the crop model. With a *DAV* of 0.74 May is the largest added value of all months. In August both simulations overestimate the the higher temperature quantiles, but while CTRL underestimates the middle part and overestimates the lower quantiles, EXP_CROP underestimates the lower temperatures and therefore also overestimates the middle part. Therefore in August *DAV* is negative.

Maps of monthly mean temperatures differences are displayed in Figure 6. All months show a mean difference of up to +3 K and −2.5 K between CTRL and OBS. A gradient from under-to overestimation from north to south (June to August) respectively Northwest to Southeast (April) is visible. In May no underestimation is evident but an increasing overestimation from Northwest to Southeast. In most parts of Germany the simulated 2m-temperatures in April, May and August are overestimated, whereas in June significant underestimates were found in the northern regions of the country. The Alpine foreland in the Southeast displays a large overestimations throughout the entire growing season. In July, the temperature bias shows a North-South gradient: CTRL is too cold in the North and too warm in the South. In Central Germany, the bias is smaller than ±1 K. Finally, August shows a warm bias of 1–2 K in Central Germany and of 2–3 K in the South.

Such biases in WRF simulated 2m-temperature with Noah-MP were also found by Chen et al. (2019) for North America and Stergiou et al. (2021) for Central Europe and cannot be associated with a single variable. They can be the result of synoptic conditions, feedback processes and parameterizations. To name three examples: (a) from April to July, both experiments overestimate the global radiation in southern Germany and underestimate it in northern Germany (not shown); (b) in Noah-MP the vegetated fraction depends on the LAI (Niu et al., 2011), which impacts the grid cells' 2m-temperature as a results of an under-/overestimation in LAI; (c) the PBL connects the land surface state and resulting fluxes to the free atmosphere and Milovac et al. (2016) showed that therefore the feedback processes and their parameterization impact the temperature and moisture simulation.

The application of the crop growth model reduces the temperature biases. In April and May, the temperature difference between EXP_CROP and CTRL is up to −2 K in the regions that were too warm in CTRL. June, July and August show that EXP_CROP has up to 1.5 K higher temperatures in the North West, where CTRL was up to 2.5 K too cold. The application of the crop growth model causes a cooling of up to 2 K compared to CTRL, which has a mean warm bias of 3 K. In July, some smaller regions in West Germany see an enhancement of the simulated temperature warm bias by up to 1.6 K.

At this point it is also important to note that temperature biases impact simulated crop growth and vice versa. Emergence and crop growth depend to a large extent on temperature. Biases of the atmospheric temperature in the model's lowest atmospheric level propagate to the crop model and influence the pace of crop development. April shows a warm bias, which results in faster crop growth. Crops reach the maximum LAI earlier than observed. Ripening is delayed in July and August.

Note that both, CTRL and EXP_CROP show a temperature bias and in EXP_CROP the relationship between temperature bias and LAI development stages is well visible. But even though a temperature bias is still present in EXP_CROP, it is reduced with respect to CTRL as a result of higher *LH* and an intensified L-A coupling in EXP_CROP (Figures 8 and 9). The impact on the LAI is seen in EXP_CROP in Section 4.1 and discussed in Section 5.

3.3. Latent and Sensible Heat Flux

The latent heat flux is proportional to the evapotranspiration, that is, in contrast to the sensible heat flux it depends on the water vapor pressure deficit and stomatal resistance which is a function of air temperature, root

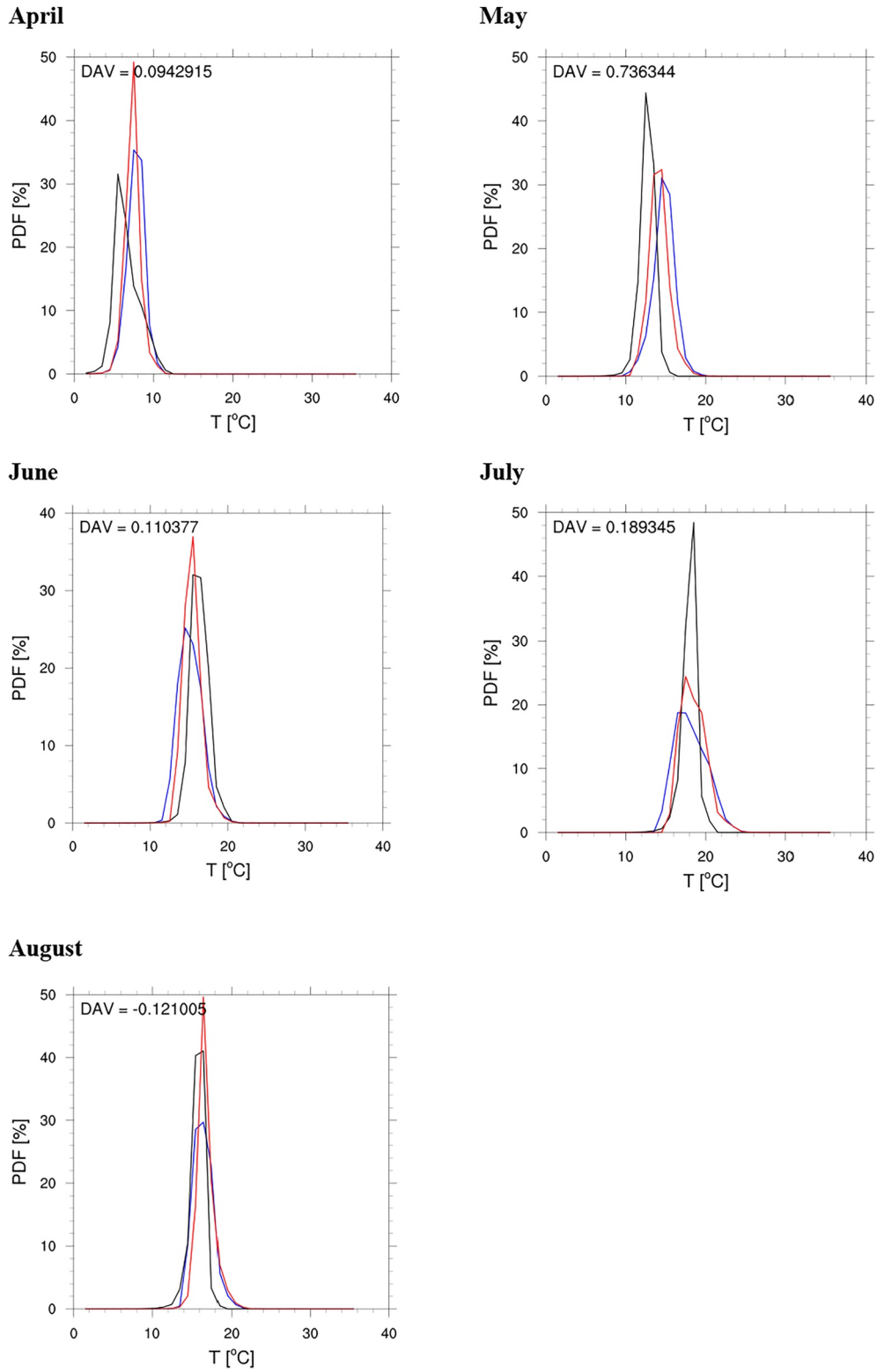

Figure 5. Distribution added value (*DAV*) and spatial probability density functions (PDF) of monthly mean temperatures of Germany for the observational data (black), control simulation (blue) and EXP_CROP (red). DAV is calculated with a binwidth of 1°C between 1°C and 36°C.

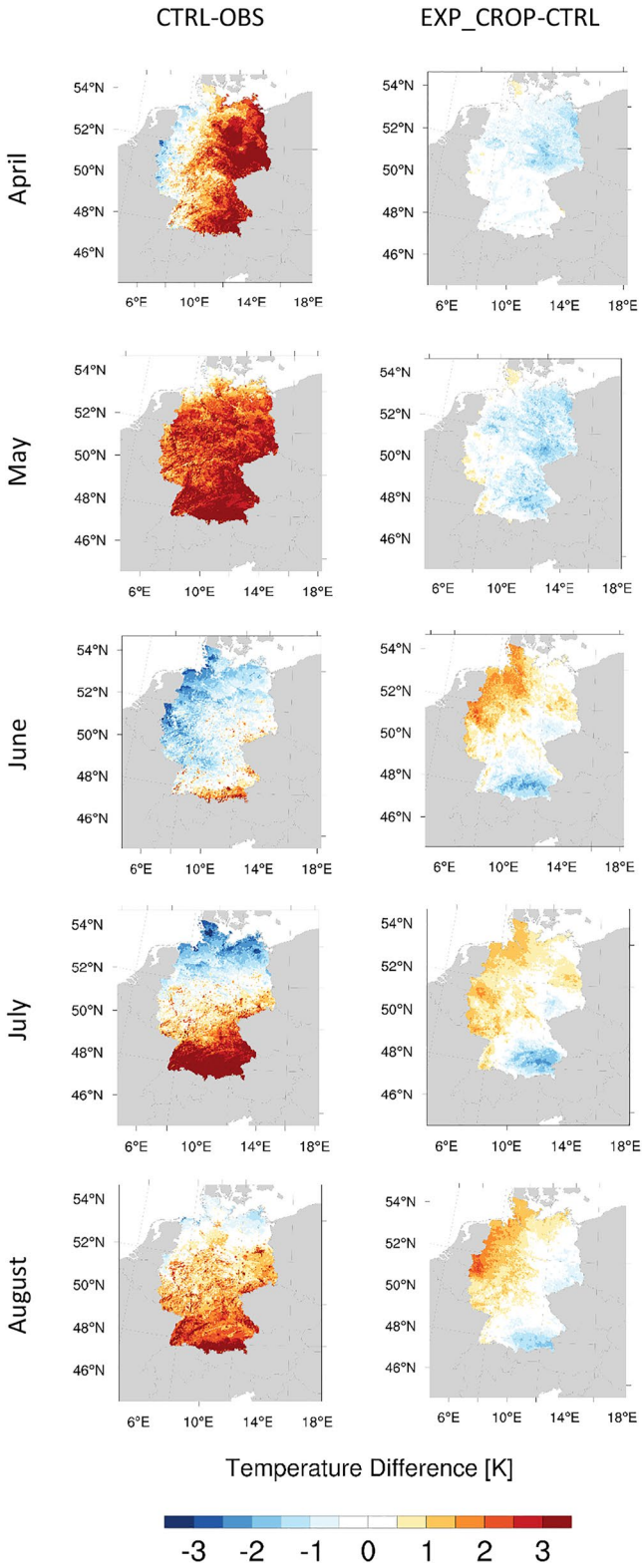

Figure 6. Differences of monthly mean temperature in 2-m height between control simulation (CTRL) and observational data (Krähenmann et al., 2016) and between EXP_CROP and CTRL.

zone soil moisture, LAI, radiation and photosynthesis. The net photosynthesis rate itself is a function of radiation, temperature, LAI, plant available water, among others. The Pearson correlation coefficient of latent and sensible heat flux is a measure of L-A coupling (Knist et al., 2017). In case of energy limiting the fluxes, the correlation is positive, in case the root zone soil moisture and LAI limit the evapotranspiration when no energy limitation is present, the correlation is small or negative with respect to L-A feedback.

Figure 7 shows the montly mean latent and sensible heat flux and their Pearson correlation coefficient for EXP_CROP and CTRL for cropland grid cells. Both experiments from April to July show an approximate North-South gradient with largest latent heat fluxes in the South and lowest in the Northwest, a gradient following the maritime to continental climate. Except for August, when the crops are partially harvested in EXP_CROP, the latent heat flux is larger in EXP_CROP than CTRL. This is in agreement with the development and magnitude of the LAI (Figures 3 and 4). The sensible heat flux shows a similar but weaker North-South gradient with significantly lower fluxes except for the southern half of Germany in August. The latent heat flux in Germany's croplands dominates over the sensible heat flux in the growing season and its stronger magnitude in EXP_CROP contributes to the cooler temperatures than in CTRL (Figures 5 and 6). The Pearson correlation coefficient shows a stronger dependence of the fluxes on the land surface conditions in EXP_CROP: During April (Figure 3), in regions with the largest LAI over central Germany the latent heat flux is limited by the stomatal resistance, while in CTRL only energy availability limits the fluxes. From May to July this is the case throughout the domain, except for some scattered regions in northern Germany in June and July. In CTRL the limitation of the latent heat from May to July flux only occurs in the regions with strong latent heat flux and is less scattered, recall that LAI and rooting depth are spatially contant in CTRL.

3.4. Terrestrial and Atmospheric Coupling Strength

The sensitivity of the *LH* variance to variations in η of the land surface model is expressed by a positive *TCI* (see Equation 3), that is, which is presented in Figure 8a for the main growing period. A negative *TCI* suggest that the *LH* drives variations in η but does not express feedback on the atmosphere (Dirmeyer, 2011). In CTRL, the terrestrial coupling is only existent south of 51°N, and moreover the values are mostly between 5 and 15 W/m^2. EXP_CROP shows significant *TCI* values of more than 10 W/m^2 south of 52°N except in the orographic terrain (see Figure 1) of the low mountain ranges and the foothills of the Alps. The strongest coupling is seen south and west of the mountain range in the center of Germany and the lowlands in the South West with a *TCI* of more than 20 W/m^2. In North West Germany, which has a stronger maritime influence, and in the alpine region in South West Germany, EXP_CROP shows no sensitivity of *LH* to η variation. In general, except for North West Germany, the dynamic crop growth model enhanced the coupling of *LH* to η. Note that in EXP_CROP the rooting depth and LAI are both dynamic and dependent on the weather footprint during the growing season.

The sensitivity of maximum daily *CAPE* variance on daytime *LH* (between 6 and 21 UTC) variability is expressed by a positive *ACI* (Equation 4). Figure 8b show a significant atmospheric coupling strength of more than 50 W/m^2 in both simulations with maxima of more than 150 W/m^2 in the

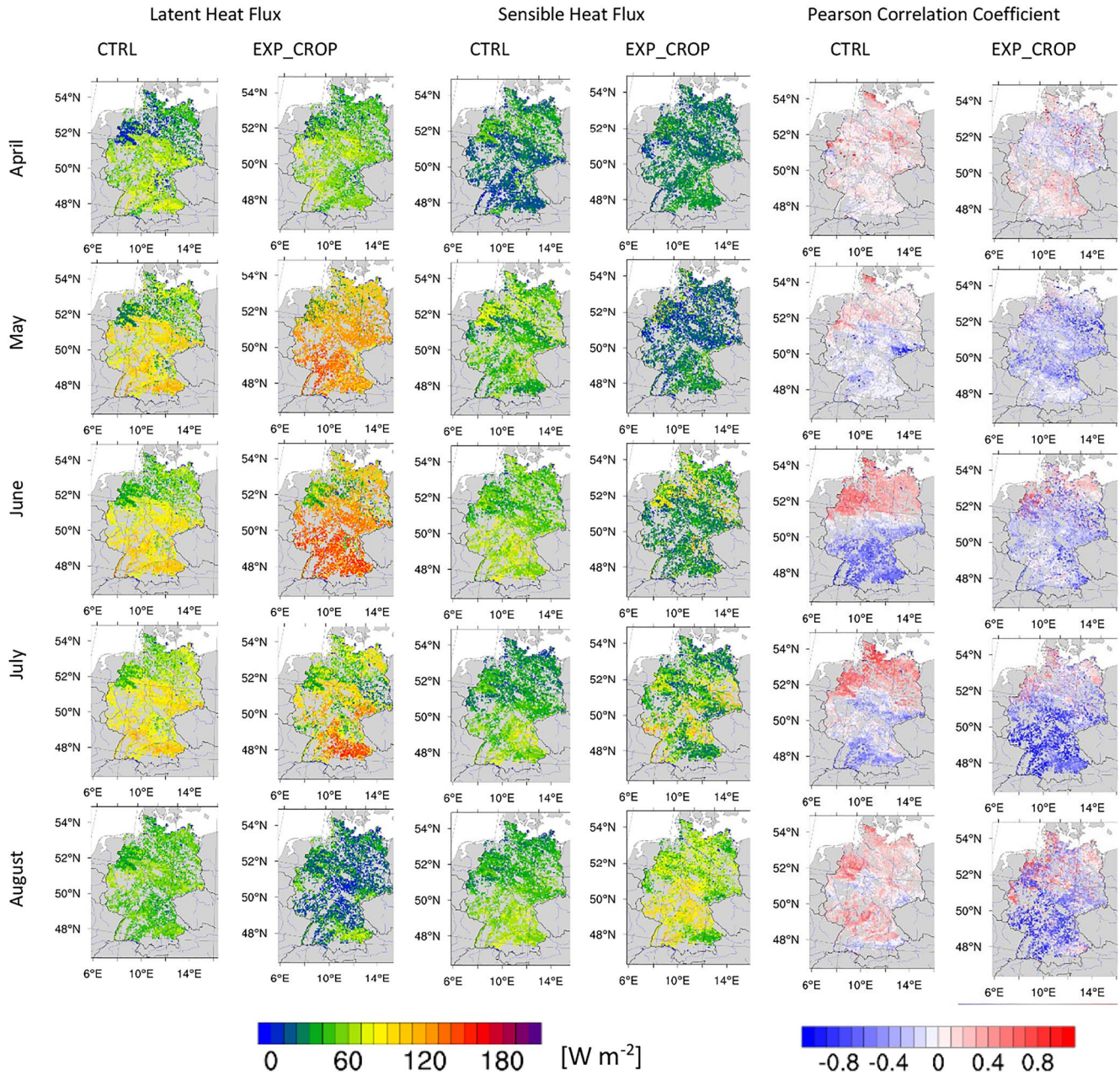

Figure 7. Monthly mean latent and sensible heat flux and their Pearson correlation coefficient in cropland grid cells of Germany in EXP_CROP and control simulation (CTRL). Non-cropland grid cells in Germany are in gray.

inland cropland regions between 48°N and 52°N and 8°E and 13°E. EXP_CROP shows a stronger atmospheric coupling than CTRL. Note that strong *ACI* coincides with large *TCI* in both simulations. Further, EXP_CROP shows a strong *ACI* in South-Eastern Germany.

Combining the terrestrial and atmospheric segment of the L-A coupling results in the *TLCI* (see Equation 5), which describes the sensitivity of daily maximum *CAPE* variance on η variation via the daytime *LH* variation. Positive values result from an impact of soil moisture via latent heat fluxes on *CAPE* showing the full coupling path between the terrestrial and atmospheric segment. Negative values occur due to the negative *TCI* and therefore suggest that LH variation impacts the soil moisture variation but this does not feed back to the atmosphere. Figure 8c shows pronounced L-A coupling in regions where *ACI* maxima coincide with *TCI* maxima (Figures 8a and 8b). North of 51°N CTRL shows no coupling between η variation and *CAPE* via *LH*. Only between 49°N and

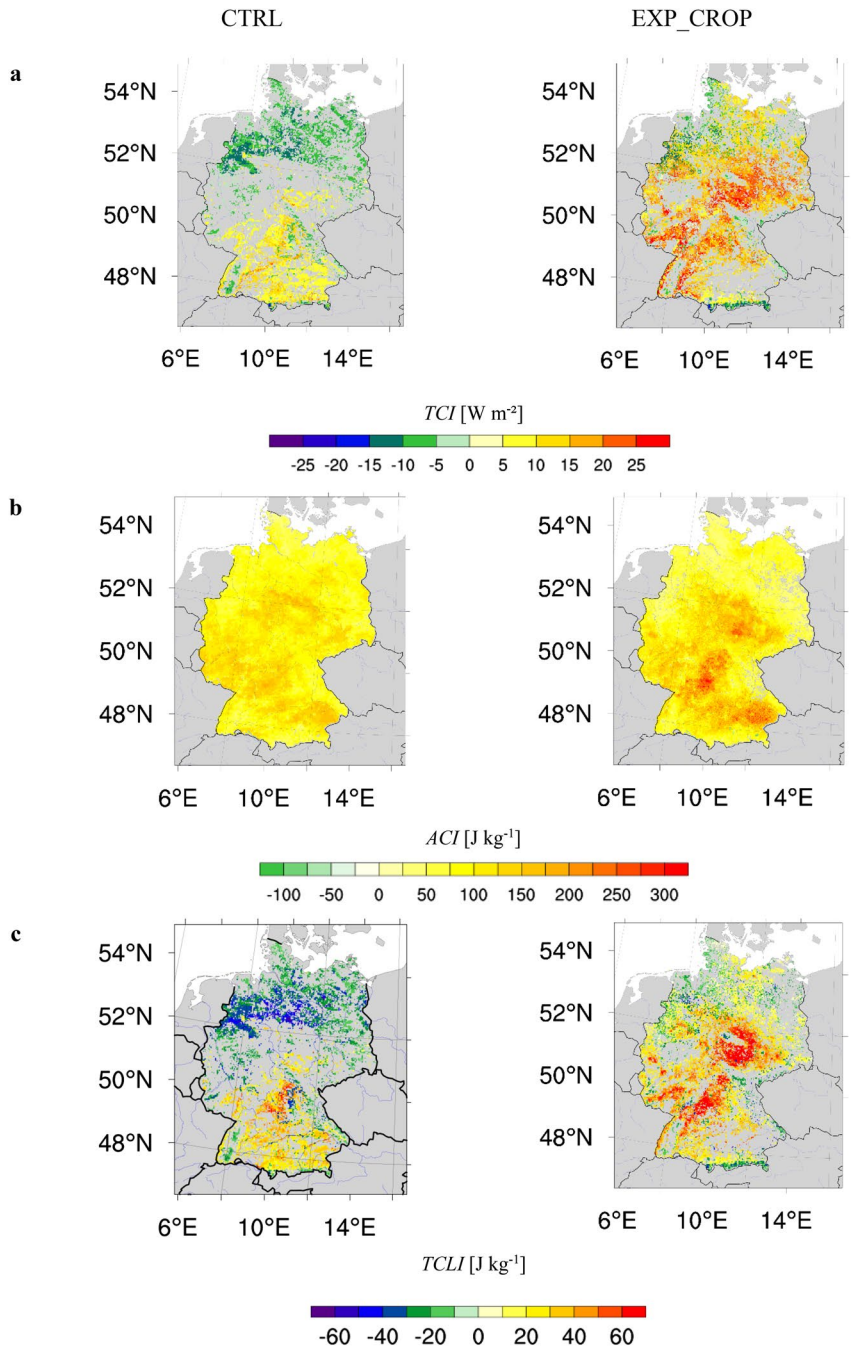

Figure 8. Coupling index based on daily data from April–August 2005 for (a) Terrestrial Coupling Index (*TCI*) for the sensitivity of the latent heat flux to variations in soil moisture; (b) Atmospheric Coupling Index (*ACI*) for the sensitivity of the *CAPE* to variations in daytime (6–21 UTC) *LH*; (c) two-legged coupling index (*TLCI*) for the sensitivity of the convective available potential energy (CAPE) to variations in soil moisture via daytime (6–21 UTC) *LH* based on daily data from April–August 2005. Positive values indicate coupling strength. Inside Germany non-significant grid cells are in gray.

51°N as well as 9°E and 11°E *TCLI* shows values above 40 W/m^2. In EXP_CROP only the North Sea coast in the North West and the Alpine region in the South do not show any L-A coupling via these metrics. Thus, except for the maritime North West and mountain ranges, the inclusion of the crop model turns regions with no L-A coupling on this path in CTRL into regions with positive coupling strength in EXP_CROP.

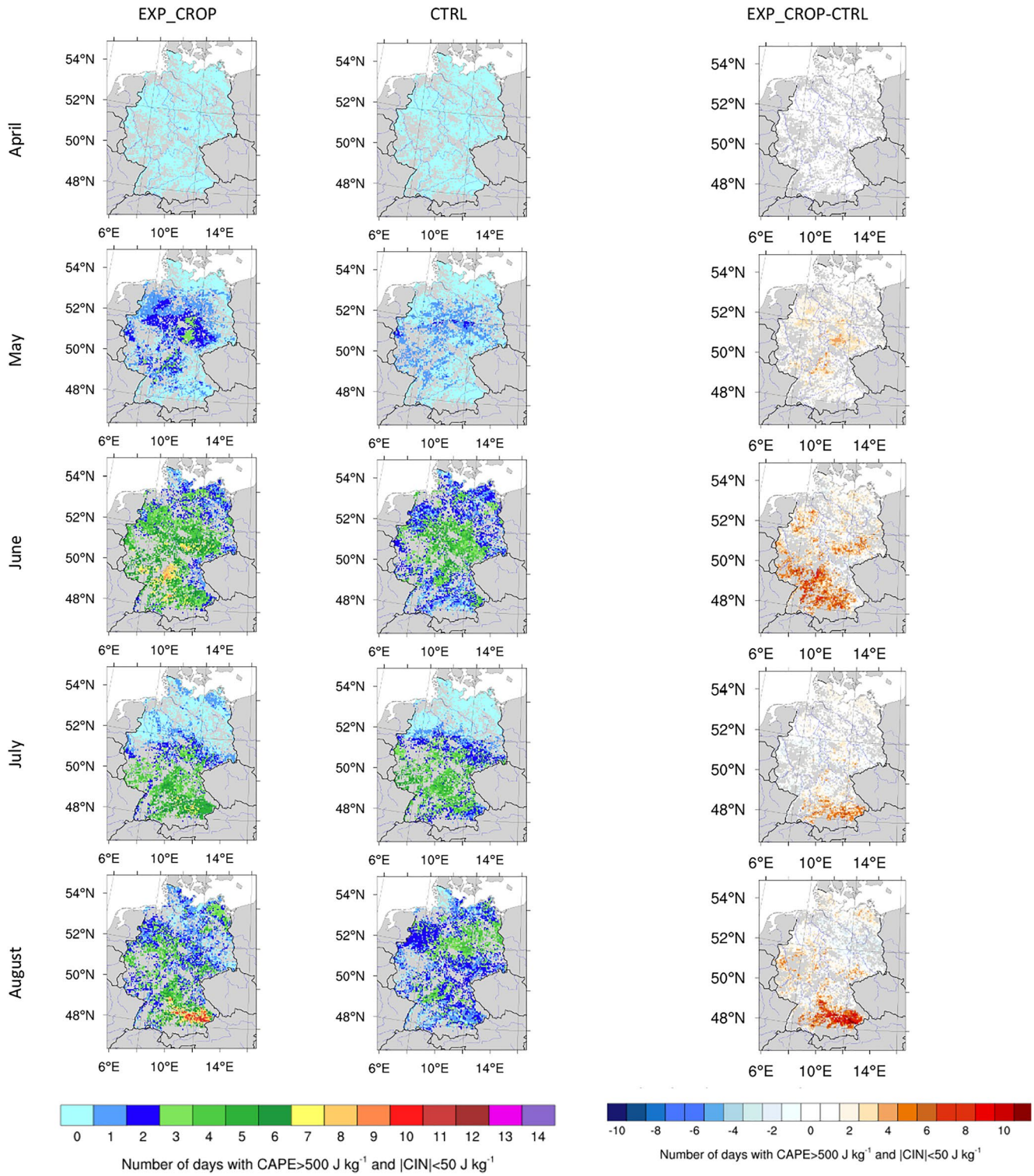

Figure 9. Number of days per month when at the same time of the day the threshold values of |*CIN*| < 50 J/kg and *CAPE* > 500 J/kg occur in EXP_CROP and control simulation (CTRL) and their difference for cropland grid cells in Germany. Non-cropland grid cells in Germany are in gray.

While *CAPE* is a measure for the potential of the occurrence of convection, convection inhibition (*CIN*) is a measure for capping deep convection. In case |*CIN*| is smaller than 50 J/kg and *CAPE* is larger than 500 J/kg, the capping of convection is weak and the atmosphere is at least marginally unstable. Figure 9 shows the number

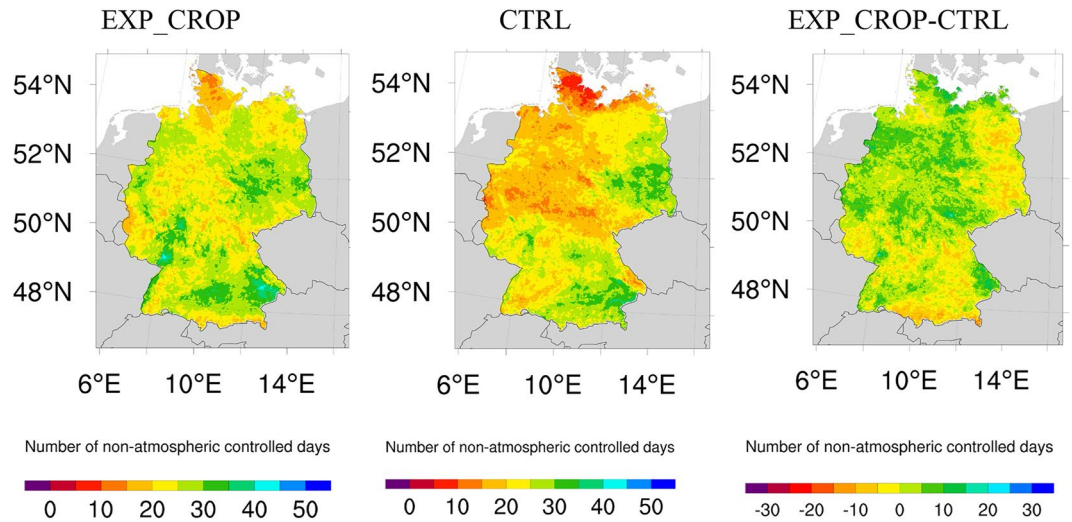

Figure 10. Non-atmospherically controlled (*nAC*) days in EXP_CROP and control simulation (CTRL) and their difference.

of days per month when at the same time of the day these threshold values are met and therefore indicates deep convection occurrence in cropland grid cells. In EXP_CROP general more days occur in the more continental climate of southern Germany than in the maritime climate in the North which is in agreement with Rüdisühli et al. (2020). CTRL only shows this gradient in July. From June to August depending on the region 4 to 11 more such days occur in EXP_CTRL than in CRTL with maxima in Bavaria (Southeast) in August. The regions coincide with larger coupling indices (Figure 8) in EXP_CROP and CTRL.

Figure 10 shows the number of *nAC* days between April and August 2005 for both simulations supporting the findings from the coupling indices. In eastern and southern Germany away from mountain ranges and the coasts CTRL shows 20–40 *nAC* days, in western and central Germany they are between 10 and 25. The inclusion of the crop-model increases the number of *nAC* in most of the domain by at least 10 days. A few regions with more than 25 *nAC* days in CTRL show a decrease by 5–10 days.

4. Discussion

Surface energy and water fluxes depend on the state of the atmospheric boundary layer (especially temperature and moisture gradients), soil (moisture, temperature) and vegetation (especially LAI and rooting depth). The atmosphere controls the photosynthesis and transpiration and therefore phenological development mainly via the radiation, temperature, humidity and wind speed. The surface water and energy balance determines the soil moisture and leads to an indirect control of photosynthesis by the atmosphere: in case of soil moistures below field capacity root water uptake is restricted by soil water content in the root zone. Summarizing this means that the phenological development impacts and depends on the L-A feedback. In CTRL the phenological cycle of crops depends on the seasonal cycle only while in EXP_CROP for early covering crops it is simulated in dependence of the atmospheric and soil state. The crops were drilled in autumn and emerged before their dormancy period in winter. This allowed for an early start of crop growth in spring once the temperatures were reaching a threshold value.

In this study, the local L-A coupling was quantified for CTRL and EXP_ CROP by analyzing *TCI*, *ACI* and *TCLI* based on η, *LH* and *CAPE*. The variables η, *LH* and *CAPE* reflect non-linear relationships between weather dependent vegetation properties (stomatal resistance, LAI and rooting depth), soil state (moisture and temperature) and the weather itself (radiation, precipitation, pressure, wind, humidity profiles, temperature profiles). In EXP_CROP, the crop development stages, that is, tillering, stem elongation, booting, flowering, ripening and senescence, depend on the temperature while the biomass production and therefore root growth and LAI depend on the photosynthesis, which depends on the stomatal resistance. The stomatal resistance depends on η and the atmospheric properties and stability in the surface layer and controls *LH* in case of soil water limitation. The inclusion of a crop growth model that is capable of simulating the LAI development in dependence of the

weather, does not only impact the terrestrial segment of the L-A coupling but also the atmospheric segment. In regions that are less impacted by maritime climate conditions in spring and summer, the variation in η impacts the *LH* and *CAPE* sensitivities. For southern Germany this is also visible in CTRL, but less pronounced. Especially the LoCo hot spot areas with respect to the η – *LH* – *CAPE* process chain in central Germany are not captured by CTRL (Figures 7 and 8). A reason is the significantly underestimated LAI in CTRL (Figures 3 and 4) and a constant rooting depth, both impacting the η – *LH* relationship in non-water limited conditions. The crop growth in EXP_CROP does not only determine LAI development but includes dynamical root growth which impacts the water fluxes and hence *LH*. The importance of considering root growth in Noah-MP has been demonstrated by Gayler et al. (2014). Further the analyses of *nAC* which is based on the atmospheric stability in dependence of the land surface state supports the results: the phenological dynamics in LAI and rooting depth in cropland increase the number of days with local L-A feedback. Jach et al. (2020) found for Mid-Europe for summer 1986–2015 that nAC days have a higher probability for precipitation than atmospherically controlled days. CTRL showed in most regions 25%–50% less nAC days than EXP_CROP, highlighting the importance of a dynamic LAI and root depth.

Gradients in the phenological phases caused by North-to-South climate and altitude variations as well as the warm Rhine valley imprint on the results of EXP_CROP. EXP_CROP simulates the weather dependent and therefore spatially heterogeneous seasonal cycle of the cropland LAI in Germany, while CTRL shows a static seasonal cycle in LAI and therefore no spatial heterogeneity. CTRL significantly underestimates the LAI and does not simulate its decline in July and August. EXP_CROP in general simulates the observed maxima and the increase and decline of the LAI, though LAI increase is too fast in April and May and declines in most regions too late and therefore not as gradual as observed in July and August.

The current model limitation of WRF-Noah-MP-Gecros to simulate the effective LAI of the grid cells can be addressed by further development of the crop growth model for more crops and crop rotations. A greater detail in crop specification/classification should also go along with a higher spatial resolution, either by lower grid cell size (at least down to a typical plot size of 2–5 ha in Western Germany) or by a tile approach in order to capture the high spatial fragmentation of (not only) Western European agriculture.

A known issue basically in all RCM simulations that do not use data assimilation is the internal variability when it comes to quantifying changing signals (Giorgi & Bi, 2000). This can be addressed via an ensemble of simulations and/or multiple years. Lavin-Gullon et al. (2021) studied the internal variability versus multi-physics uncertainty for convection permitting simulations in central Europe with WRF. They found "for near-surface temperature the spread associated to parameterizations was above that due to the internal variability," the variable is rather constrained by the model physics than the internal variability. The scope of this study is the presentation of WRF-Noah-MP-Gecros and its general impact on L-A feedback. In Germany the weather is temporally and spatially very variable, so that many meteorological conditions occur, especially in the season from April to August, which is particularly important for the L-A exchange. Winter wheat is very well simulated with Noah-MP-Gecros in its development as a function of weather (Ingwersen et al., 2018). This is enhanced in this study with WRF-Noah-MP-Gecros where the atmosphere reacts to this plant growth in EXP_CROP and this affects the growth accordingly. The goal here is to study if this enhances L-A-feedback. Further studies will be required to quantify the long-term L-A feedback with an ensemble of multi-year simulations and multi-physics ensembles (e.g., including different PBL and surface layer schemes) as well as OBS.

It is important to study and to verify L-A feedback metrics advanced observations in the future. Novel synergies of instrumentation (Späth et al., 2016; Wulfmeyer et al., 2018) provide not only surface state and surface flux measurements but also the necessary atmospheric profiles, gradients, and turbulent moments of tempe-rature, moisture and wind (Behrendt et al., 2019) to understand and quantify the LoCo process chain (Santanello et al., 2018). Implementation of such observati-on systems at observatories such as the L-A Feedback Observatory (LAFO, https://lafo.uni-hohenheim.de/en) in Stuttgart (Germany) allows for the validation of the L-A feedback in models, since this requires multi-year data during the main growing season for multiple crops due to their large variability in weather responses (Ingwersen et al., 2011; Wizemann et al., 2014). GEWEX Land Atmosphere Feedback Observatories have also been introduced and proposed to be operated in other climate regions (Wulfmeyer et al., 2020).

5. Conclusions

Weather and climate in the mid-latitudes of the northern hemisphere widely depends on L-A interaction. The landscape is heterogeneous due to different soil properties and land cover as well as due to orography. Land use and land cover changes are getting increasing attention in global and regional climate change modeling due to their impact on regional climate. Studies by Branch and Wulfmeyer (2019), Kumar et al. (2013), Lejeune et al. (2017) and Noblet-Ducoudré et al. (2012) confirm the impact of land use and land cover on the climate and therefore temperatures. While global climate models in Coupled Model Intercomparison Project Phases 5 and 6 (CMIP5, CMIP6) simulations include biogeochemical land surface models with weather dependent vegetation dynamics Arora et al. (2020) and Huang et al. (2016), this is not yet state of the art in RCMs (Davin et al., 2019).

Agricultural croplands show a weather dependent annual cycle of vegetation character-istics such as LAI, GVF, and rooting depth. Current state of the art RCMs apply fixed annual cycles of vegetation characteristics, which cause biases in surface fluxes and incorrect representation of L-A feedback and errors in atmospheric variables and PBL evolution. This study implemented an advanced vegetation parameterization represented by Gecros model inside of Noah-MP for croplands with winter wheat in Germany (Ingwersen et al., 2018). By conducting a 1-year impact study with the coupled WRF-Noah-MP-Gecros model (EXP_CROP), we demonstrated a strengthening of L-A feedback comparing to WRF-Noah-MP with the default static seasonal LAI cycle (CTRL). Its strength was analyzed for the process chain of η, *LH* and *CAPE* applying the terrestrial, atmospheric and two-legged coupling indices.

Regions that did not show any L-A feedback in CTRL, showed emerging feedback between the η, *LH* and *CAPE* in EXP_CROP.This also resulted in more days with an unstable atmosphere and weakened convection inhibition especially during summer. Except for the maritime North West and mountain ranges, the inclusion of the crop model turns regions with no L-A coupling on this path into regions with positive coupling. Our work shows that the impact is positive and results in a bias reduction on the local monthly mean temperature, depending on the month and region biases reduce by up to 2–3 K. Except for August the monthly temperature *DAV* improves in EXP_CROP.

These results of the simulations confirm that for seasonal and climate simulations it is crucial to simulate a weather-driven crop development due to its significant impact on L-A coupling. Given this information in the mid to long term, farmers might be able to adapt crop choice to help mitigate changing environmental stresses. The sensitivity of the L-A coupling and therefore climate to crop growth calls for the implementation of more crops and crop management (sowing dates, sowing density, N fertilization etc.) with intense cooperation with the crop modeling community to derive the necessary parameter sets.

More important for future convection-permitting seasonal and climate simulations in cropland dominated regions, our simulations results show that the implementation of a crop growth model leads to:

- Spatially heterogeneous crop development (Figure 3)
- Higher LAI values and a stronger pronounced LAI seasonality (Figures 3 and 4)
- Declining LAI values during the ripening and harvest periods (Figures 3 and 4)
- Intensified L-A coupling (Figures 7 and 8)
- More days with conditions for deep convection (Figure 9)

and

- A significant bias reduction of monthly mean temperatures (Figure 5).

This study's implementation of the crop model Gecros was released with WRF version 4, which enables the simulation of the annual phenological development of croplands in a changing climate when downscaling CMIP6 climate projections in the future. This is crucial for the regional climate simulations in mid-latitudes due to the L-A feedback processes and the currently observed and expected future change in phenological phases.

Conflict of Interest

The authors declare no conflicts of interest relevant to this study.

Data Availability Statement

The Copernicus Climate Change Service information (2018) satellite derived LAI was compared with used to evaluate the model simulations in croplands is freely available at https://cds.climate.copernicus.eu/ via download. The gridded observed daily 2m-temperature OBS used for evaluation of the model simulations is freely available at the climate data center of the German Weather Service via download from https://opendata.dwd.de/climate_environment/CDC/grids_germany/daily/Project_TRY/air_temperature_mean/ and described by Krähenmann et al. (2016). The simulations CTRL and EXP_CROP required forcing data. We used our 3-hourly (Tier2) data from the 0.11° grid WRF simulations forced with ERA-Interim reanalysis data (Dee et al., 2011). These simulation data sets (CTRL, EXP_CROP and the forcing data) are very large, they can be made available by request from the corresponding author. The namelist.input file for the WRF simulations and analyzed variables (temperature, *LH, SH, CAPE, CIN, LAI, nAC*) from CTRL and EXP_CROP are available at the depository Zenodo via https://doi.org/10.5281/zenodo.6501984 (Warrach-Sagi, 2022). Weather Research and Forecasting version 3.7.1 was used for CTRL and EXP_CROP. The WRF source code can be obtained from http://www2.mmm.ucar.edu/wrf/users/download/get_source.html after registration. The applied WRF version 3.7.1 code changes for Gecros can be obtained upon request from the corresponding author. The land cover was based on the CLC 2006 data (http://land.copernicus.eu/pan-european/corine-land-cover/clc-2006/view), which was reclassified into the IGBP-MODIS land cover types applied by WRF (Bauer et al., 2020). The applied soil texture data is based on the Harmonized World Soil Database (version 1.21) and available from the World Data Center for Climate (https://doi.org/10.1594/WDCC/WRF_NOAH_HWSD_world_TOP_SOILTYP, Milovac et al. (2018)). The software package NCL (Brown et al., 2012) was applied for the figures and the calculation of the Pearson correlation coefficients and can be downloaded from https://www.ncl.ucar.edu/. The climate data operator software is freely available at https://code.mpimet.mpg.de/projects/cdo/files and described by Schulzweida (2019). The Coupling Metrics Toolkit (CoMeT; https://www.coupling-metrics.com) is an open-source code package (Santanello et al., 2018), we used it to calculate the coupling indices *TCI, ACI* and *TLCI*.

Acknowledgments
We gratefully acknowledge the financial support by the German Research Foundation (DFG) in the frame of the Research Unit 1695 "Agricultural Landscapes under Global Climate Change – Processes and Feedbacks on a Regional Scale." The simulations have been carried out at the High-Performance Computing Center Stuttgart (HLRS) on the Cray XC40 Hazel Hen. We thank the anonymous reviewers for their helpful comments that helped to improve this paper. Open Access funding enabled and organized by Projekt DEAL.

References

Arora, V. K., Katavouta, A., Williams, I. N., Jones, C. D., Brovkin, V., Friedlingstein, P., et al. (2020). Carbon-concentration and carbon-climate feedbacks in CMIP6 models, and their comparison to CMIP5 models. *Biogeosciences*, *17*, 4173–4222. https://doi.org/10.5194/bg-17-4173-2020

Asseng, S., Ewert, F., Rosenzweig, C., Jones, J. W., Hatfield, J. L., Ruane, A. C., et al. (2013). Uncertainty in simulating wheat yields under climate change. *Nature Climate Change*, *3*(9), 827–832. https://doi.org/10.1038/nclimate1916

Bauer, H.-S., Muppa, S. K., Wulfmeyer, V., Behrendt, A., Warrach-Sagi, K., & Späth, F. (2020). Multi-nested WRF simulations for studying planetary boundary layer processes on the turbulence-permitting scale in a realistic mesoscale environment. *Tellus A: Dynamic Meteorology and Oceanography*, *72*(1), 1–28. https://doi.org/10.1080/16000870.2020.1761740

Becker, K., Wulfmeyer, V., Berger, T., Gebel, J., & Münch, W. (2013). Carbon farming in hot, dry coastal areas: An option for climate change mitigation. *Earth System Dynamics*, *4*(2), 237–251. https://doi.org/10.5194/esd-4-237-2013

Behrendt, A., Wulfmeyer, V., Senff, C., Muppa, S. K., Späth, F., Lange, D., & Kalthoff, N. (2019). Observation of sensible and latent heat flux profiles with lidar. *Atmospheric Measurement Techniques*. https://doi.org/10.5194/amt-2019-305

Biernath, C., Gayler, S., Bittner, S., Klein, C., Högy, P., Fangmeier, A., & Priesack, E. (2011). Evaluating the ability of four crop models to predict different environmental impacts on spring wheat grown in open-top chambers. *European Journal of Agronomy*, *35*(2), 71–82. https://doi.org/10.1016/j.eja.2011.04.001

BMEL. (2017). Daten und Fakten Land-, Forst- und Ernährungswirtschaft mit Fischerei und Wein- und Gartenbau. Retrieved from https://www.bmel.de/SharedDocs/Downloads/DE/Broschueren/Daten-und-Fakten-Landwirtschaft.html

Bohm, K., Ingwersen, J., Milovac, J., & Streck, T. (2019). Distinguishing between early and late covering crops in the land surface model Noah-MP: Impact on simulated surface energy fluxes and temperature. https://doi.org/10.5194/bg-17-2791-2020

Branch, O., & Wulfmeyer, V. (2019). Deliberate enhancement of rainfall using desert plantations. *Proceedings of the National Academy of Sciences of the United States of America*, (Vol. 116(38), pp. 18841–18847). https://doi.org/10.1073/pnas.1904754116

Brown, D., Brownrigg, R., Haley, M., & Huang, W. (2012). NCAR command language (NCL). NCL, [Software]. https://doi.org/10.5065/D6WD3XH5

Bülow, K., Hübener, H., Keuler, K., Menz, C., Pfeifer, S., Ramthun, H., et al. (2019). User tailored results of a regional climate model ensemble to plan adaption to the changing climate in Germany. *Advances in Science and Research*, *16*, 241–249. https://doi.org/10.5194/asr-16-241-2019

Camacho, F., Cernicharo, J., Lacaze, R., Baret, F., & Weiss, M. (2013). GEOV1: LAI, FAPAR essential climate variables and FCOVER global time series capitalizing over existing products. Part 2: Validation and intercomparison with reference products. *Remote Sensing of Environment*, *137*, 310–329. https://doi.org/10.1016/j.rse.2013.02.030

Chen, F., Li, Y., Barlage, M., Zhang, Z., & Li, Z. (2019). Using 4-km WRF CONUS simulations to assess impacts of the surface coupling strength on regional climate simulation. *Climate Dynamics*, *53*(9–10), 6397–6416. https://doi.org/10.1007/s00382-019-04932-9

Collins, W., Rasch, P., Boville, B., McCaa, J., Williamson, D., Kiehl, J., et al. (2004). Description of the NCAR community atmosphere model (CAM 3.0). Retrieved from https://www.cesm.ucar.edu/models/atm-cam/docs/description/description.pdf

CoMeT, C. (2016). Metrics Toolkit Coupling Metrics [Software]. Retrieved from https://www.coupling-metrics.com

Copernicus Climate Change Service information. (2018). Leaf area index and fraction absorbed of photosynthetically active radiation 10-daily gridded data from 1998 to present, SPOT/VEGETATION v1.0. [Dataset]. Advances in Contraceptive Delivery System. Retrieved from https://cds.climate.copernicus.eu/

Coppola, E., Sobolowski, S., Pichelli, E., Raffaele, F., Ahrens, B., Anders, I., et al. (2018). A first-of-its-kind multi-model convection permitting ensemble for investigating convective phenomena over Europe and the Mediterranean. *Climate Dynamics*, *42*(7–8), 3–34. https://doi.org/10.1007/s00382-018-4521-8

Davin, E., Rechid, D., Breil, M., Cardoso, R. M., Coppola, E., Hoffmann, P., et al. (2019). Biogeophysical impacts of forestation in Europe: First results from the LUCAS regional climate model intercomparison. *Earth System Dynamics Discussions*, 1–31. https://doi.org/10.5194/esd-2019-4

Dee, D. P., Uppala, S. M., Simmons, A. J., Berrisford, P., Poli, P., Kobayashi, S., et al. (2011). The ERA-interim reanalysis: Configuration and performance of the data assimilation system. *Quarterly Journal of the Royal Meteorological Society*, *137*(656), 553–597. https://doi.org/10.1002/qj.828

Dirmeyer, P. A. (2011). The terrestrial segment of soil moisture-climate coupling. *Geophysical Research Letters*, *38*(16). https://doi.org/10.1029/2011GL048268

Dirmeyer, P. A., Cash, B. A., Kinter, J. L., Stan, C., Jung, T., Marx, L., et al. (2012). Evidence for enhanced land–atmosphere feedback in a warming climate. *Journal of Hydrometeorology*, *13*(3), 981–995. https://doi.org/10.1175/JHM-D-11-0104.1

Dirmeyer, P. A., Wang, Z., Mbuh, M. J., & Norton, H. E. (2014). Intensified land surface control on boundary layer growth in a changing climate. *Geophysical Research Letters*, *41*(4), 1290–1294. https://doi.org/10.1002/2013GL058826

DWD. (2019). Zeitreihen und Trends von Gebietsmitteln der Parameter Temperatur, Niederschlag, Sonnenscheindauer und verschiedener Kenntage. Retrieved from https://www.dwd.de/EN/ourservices/zeitreihen/zeitreihen.html

Findell, K. L., & Eltahir, E. A. B. (2003). Atmospheric controls on soil moisture–boundary layer interactions. Part I: Framework development. *Journal of Hydrometeorology*, *4*(3), 552–569. https://doi.org/10.1175/1525-7541(2003)004%3C0552:ACOSML%3E2.0.CO;2

Fuster Ochando, B., & Sánchez-Zapero, J. (2019). Product quality assessment report CDR VGT-based LAI and FAPAR v1.0. Retrieved from https://datastore.copernicus-climate.eu/documents/satellite-lai-fapar/D2.3.7-v1.0_PQAR_CDR_LAI_FAPAR_SPOT-VGT_v1.0_PRODUCTS_v1.0.pdf

Gayler, S., Wöhling, T., Grzeschik, M., Warrach-Sagi, K., Attinger, S., Streck, T., et al. (2014). Incorporating dynamic root growth enhances the performance of Noah-MP at two contrasting winter wheat field sites. *Water Resources Research*, *50*(2), 1337–1336. https://doi.org/10.1002/2013WR014634

Giorgi, F., & Bi, X. (2000). A study of internal variability of a regional climate model. *Journal of Geophysical Research*, *105*(D24), 29503–29521. https://doi.org/10.1029/2000JD900269

Goudriaan, J., & van Laar, H. H. (1994). Modelling potential crop growth processes: Textbook with exercises. In *Current issues in production ecology: Vol. 2*. Kluwer Acad. Publ.

Guo, Z., Dirmeyer, P. A., Koster, R. D., Sud, Y. C., Bonan, G. B., Oleson, K. W., et al. (2006). GLACE: The global land–atmosphere coupling experiment. Part II: Analysis. *Journal of Hydrometeorology*, *7*(4), 611–625. https://doi.org/10.1175/JHM511.1

Harding, K. J., Twine, T. E., & Lu, Y. (2015). Effects of dynamic crop growth on the simulated precipitation response to irrigation. *Earth Interactions*, *19*(14), 1–31. https://doi.org/10.1175/EI-D-15-0030.1

Högy, P., Kottmann, L., Schmid, I., & Fangmeier, A. (2019). Heat, wheat and CO_2: The relevance of timing and the mode of temperature stress on biomass and yield. *Journal of Agronomy and Crop Science*, *205*(6), 608–615. https://doi.org/10.1111/jac.12345

Huang, Y., Gerber, S., Huang, T., & Lichstein, J. W. (2016). Evaluating the drought response of CMIP5 models using global gross primary productivity, leaf area, precipitation, and soil moisture data. *Global Biogeochemical Cycles*, *30*(12), 1827–1846. https://doi.org/10.1002/2016GB005480

Hübener, H., Hoffmann, P., Keuler, K., Pfeifer, S., Ramthun, H., Spekat, A., et al. (2017). Deriving user-informed climate information from climate model ensemble results. *Advances in Science and Research*, *14*, 261–269. https://doi.org/10.5194/asr-14-261-2017

Imukova, K., Ingwersen, J., & Streck, T. (2015). Determining the spatial and temporal dynamics of the green vegetation fraction of croplands using high-resolution RapidEye satellite images. *Agricultural and Forest Meteorology*, *206*, 113–123. https://doi.org/10.1016/j.agrformet.2015.03.003

Ingwersen, J., Högy, P., Wizemann, H.-D., Warrach-Sagi, K., & Streck, T. (2018). Coupling the land surface model Noah-MP with the generic crop growth model Gecros: Model description, calibration and validation. *Agricultural and Forest Meteorology*, *262*, 322–339. https://doi.org/10.1016/j.agrformet.2018.06.023

Ingwersen, J., Steffens, K., Poltoradnev, M., Gäbler, R., Streck, T., Högy, P., et al. (2011). Comparison of Noah simulations with eddy covariance and soil water measurements at a winter wheat stand. *Agricultural and Forest Meteorology*, *151*(3), 345–344. https://doi.org/10.1016/j.agrformet.2010.11.010

Ivanov, M., Warrach-Sagi, K., & Wulfmeyer, V. (2018a). Field significance of performance measures in the context of regional climate model evaluation. Part 1: Temperature. *Theoretical and Applied Climatology*, *132*(1–2), 219–237. https://doi.org/10.1007/s00704-017-2100-2

Ivanov, M., Warrach-Sagi, K., & Wulfmeyer, V. (2018b). Field significance of performance measures in the context of regional climate model evaluation. Part 2: Precipitation. *Theoretical and Applied Climatology*, *132*(1–2), 239–238. https://doi.org/10.1007/s00704-017-2077-x

Jach, L., Warrach-Sagi, K., Ingwersen, J., Kaas, E., & Wulfmeyer, V. (2020). Land cover impacts on land-atmosphere coupling strength in climate simulations with WRF over Europe. *Journal of Geophysical Research: Atmospheres*, *125*(18), e2019JD031989. https://doi.org/10.1029/2019JD031989

Jacob, D., Teichmann, C., Sobolowski, S., Katragkou, E., Anders, I., Belda, M., et al. (2020). Regional climate downscaling over Europe: Perspectives from the EURO-CORDEX community. *Regional Environmental Change*, *20*, 51. https://doi.org/10.1007/s10113-020-01606-9

Knist, S., Simmer, C., Goergen, K., Buonomo, E., Christensen, O. B., Colette, A., et al. (2017). Land-atmosphere coupling in EURO-CORDEX evaluation experiments. *Journal of Geophysical Research*, *122*(1), 79–78. https://doi.org/10.1002/2016JD025476

Kotlarski, S., Lüthi, D., Schär, C., Keuler, K., Christensen, O. B., Colette, A., et al. (2014). Regional climate modeling on European scales: A joint standard evaluation of the EURO-CORDEX RCM ensemble. *Geoscientific Model Development*, *7*(4), 1297–1296. https://doi.org/10.5194/gmd-7-1297-2014

Krähenmann, S., Walter, A., Brienen, S., Imbery, F., & Matzarakis, A. (2016). Monthly, daily and hourly grids of 12 commonly used meteorological variables for Germany estimated by the Project TRY Advancement [Dataset]. CDC. Retrieved from https://opendata.dwd.de/climate_environment/CDC/grids_germany/daily/Project_TRY/air_temperature_mean/

Kumar, S., Dirmeyer, P. A., Merwade, V., DelSole, T., Adams, J. M., & Niyogi, D. (2013). Land use/cover change impacts in CMIP5 climate simulations: A new methodology and 21st century challenges. *Journal of Geophysical Research: Atmospheres*, *118*(12), 6337–6353. https://doi.org/10.1002/jgrd.50463

Lavin-Gullon, A., Fernandez, J., Bastin, S., Cardoso, R. M., Fita, L., Giannaros, T. M., et al. (2021). Internal variability versus multi-physics uncertainty in a regional climate model. *International Journal of Climatology*, *41*(S1). https://doi.org/10.1002/joc.6717

Lejeune, Q., Seneviratne, S. I., & Davin, E. (2017). Historical land-cover change impacts on climate: Comparative assessment of LUCID and CMIP5 multimodel experiments. *Journal of Climate*, *30*(4), 1439–1459. https://doi.org/10.1175/JCLI-D-16-0213.1

Liu, X., Chen, F., Barlage, M., Zhou, G., & Niyogi, D. (2016). Noah-MP-Crop: Introducing dynamic crop growth in the Noah-MP land surface model. *Journal of Geophysical Research: Atmospheres*, *121*(23), 13953–13972. https://doi.org/10.1002/2016JD025597

Lu, Y., Williams, I. N., Bagley, J. E., Torn, M. S., & Kueppers, L. M. (2017). Representing winter wheat in the community land model (version 4.5). *Geoscientific Model Development*, *10*(5), 1873–1888. https://doi.org/10.5194/gmd-10-1873-2017

Mahowald, N., Lo, F., Zheng, Y., Harrison, L., Funk, C., Lombardozzi, D., & Goodale, C. (2016). Projections of leaf area index in Earth system models. *Earth System Dynamics*, *7*(1), 211–229. https://doi.org/10.5194/esd-7-211-2016

Mahrt, L. (2000). Surface heterogeneity and vertical structure of the boundary layer. *Boundary-Layer Meteorology*, *96*(1–2), 33–62. https://doi.org/10.1023/A:1002482332477

Maronga, B., & Raasch, S. (2013). Large-eddy simulations of surface heterogeneity effects on the convective boundary layer during the LITFASS-2003 experiment. *Boundary-Layer Meteorology*, *146*(1), 17–44. https://doi.org/10.1007/s10546-012-9748-z

Milovac, J., Ingwersen, J., & Warrach-Sagi, K. (2018). Soil texture forcing data for the whole world for the Weather Research and Forecasting (WRF) Model of the University of Hohenheim (UHOH) based on the Harmonized World Soil Database (HWSD) at 30 arc-second horizontal resolution [Dataset]. WDCC. https://doi.org/10.1594/WDCC/WRF_NOAH_HWSD_world_TOP_SOILTYP

Milovac, J., Warrach-Sagi, K., Behrendt, A., Späth, F., Wulfmeyer, V., & Ingwersen, J. (2016). Investigation of PBL schemes combining the WRF model simulations with scanning water vapor differential absorption lidar measurements. *Journal of Geophysical Research*, *121*(2), 624–623. https://doi.org/10.1002/2015JD023927

Miralles, D. G., Gentine, P., Seneviratne, S. I., & Teuling, A. J. (2019). Land-atmospheric feedbacks during droughts and heatwaves: State of the science and current challenges. *Annals of the New York Academy of Sciences*, *1436*(1), 19–35. https://doi.org/10.1111/nyas.13912

Morrison, H., Thompson, G., & Tatarskii, V. (2009). Impact of cloud microphysics on the development of trailing stratiform precipitation in a simulated squall line: Comparison of one- and two-moment schemes. *Monthly Weather Review*, *137*(3), 991–1007. https://doi.org/10.1175/2008MWR2556.1

Myneni, R., Hoffman, S., Knyazikhin, Y., Privette, J., Glassy, J., Tian, Y., et al. (2002). Global products of vegetation leaf area and fraction absorbed PAR from year one of MODIS data. *Remote Sensing of Environment*, *83*(1–2), 214–231. https://doi.org/10.1016/S0034-4257(02)00074-3

Nakanishi, M., & Niino, H. (2009). Development of an improved turbulence closure model for the atmospheric boundary layer. *Journal of the Meteorological Society of Japan*, *87*(5), 895–912. https://doi.org/10.2151/jmsj.87.895

Niu, G.-Y., Yang, Z.-L., Mitchell, K., Chen, F., Ek, M. B., Barlage, M., et al. (2011). The community Noah land surface model with multiparameterization options (Noah-MP): 1. Model description and evaluation with local-scale measurements. *Journal of Geophysical Research*, *116*(D12), 1381. https://doi.org/10.1029/2010JD015139

Noblet-Ducoudré, N., de Boisier, J.-P., Pitman, A., Bonan, G. B., Brovkin, V., Cruz, F., et al. (2012). Determining robust impacts of land-use-induced land cover changes on surface climate over North America and Eurasia: Results from the first set of LUCID experiments. *Journal of Climate*, *25*(9), 3261–3281. https://doi.org/10.1175/JCLI-D-11-00338.1

Osborne, T. M., Lawrence, D. M., Challinor, A. J., Slingo, J. M., & WHEELER, T. R. (2007). Development and assessment of a coupled crop?-climate model. *Global Change Biology*, *13*(1), 169–183. https://doi.org/10.1111/j.1365-2486.2006.01274.x

Partridge, T. F., Winter, J. M., Kendall, A. D., & Hyndman, D. W. (2021). Cross-scale evaluation of dynamic crop growth in WRF and Noah-MP-Crop. *Agricultural and Forest Meteorology*, *296*, 108217. https://doi.org/10.1016/j.agrformet.2020.108217

Perkins, S. E., Pitman, A. J., Holbrook, N. J., & McAneney, J. (2007). Evaluation of the AR4 climate models' simulated daily maximum temperature, minimum temperature, and precipitation over Australia using probability density functions. *Journal of Climate*, *20*(17), 4356–4376. https://doi.org/10.1175/JCLI4253.1

Ritchie, J. T., Godwin, D. C., & Otter, S. (1985). *CERES-wheat: A user-oriented wheat yield model. Preliminary documentation. (No. YM-U3-04442-JSC-18892)*. Michigan State University, AGRISTARS Publication.

Rüdisühli, S., Sprenger, M., Leutwyler, D., Schär, C., & Wernli, H. (2020). Attribution of precipitation to cyclones and fronts over Europe in a kilometer-scale regional climate simulation. *Weather and Climate Dynamics*, *1*(2), 675–699. https://doi.org/10.5194/wcd-1-675-2020

Santanello, J. A., Dirmeyer, P. A., Ferguson, C. R., Findell, K. L., Tawfik, A. B., Berg, A., et al. (2018). Land–atmosphere interactions: The LoCo perspective. *Bulletin of the American Meteorological Society*, *99*(6), 1253–1272. https://doi.org/10.1175/BAMS-D-17-0001.1

Schulzweida, U. (2019). *CDO user guide (1.9.8)*. Zenodo. https://doi.org/10.5281/zenodo.3539275

Schwitalla, T., Branch, O., & Wulfmeyer, V. (2020). Sensitivity study of the planetary boundary layer and microphysical schemes to the initialization of convection over the Arabian Peninsula. *Quarterly Journal of the Royal Meteorological Society*, *146*(727), 846–869. https://doi.org/10.1002/qj.3711

Skamarock, W., Klemp, J., Dudhia, J., Gill, D., Barker, D., Wang, W., et al. (2008). A Description of the advanced research WRF version 3. http://dx.doi.org/10.5065/D68S4MVH

Soares, P. M. M., Cardoso, R. M., Lima, D. C. A., & Miranda, P. M. A. (2017). Future precipitation in Portugal: High-resolution projections using WRF model and EURO-CORDEX multi-model ensembles. *Climate Dynamics*, *49*(7–8), 2503–2530. https://doi.org/10.1007/s00382-016-3455-2

Späth, F., Behrendt, A., Muppa, S. K., Metzendorf, S., Riede, A., & Wulfmeyer, V. (2016). 3-D water vapor field in the atmospheric boundary layer observed with scanning differential absorption lidar. *Atmospheric Measurement Techniques*, *9*(4), 1701–1720. https://doi.org/10.5194/amt-9-1701-2016

Stergiou, I., Tagaris, E., & Sotiropoulou, R.-E. P. (2021). Investigating the WRF temperature and precipitation performance sensitivity to spatial resolution over Central Europe. *Atmosphere*, *12*(2), 278. https://doi.org/10.3390/atmos12020278

USDA. (2019). USDA crop production: 2018 summary. Retrieved from https://www.nass.usda.gov/Publications/Todays_Reports/reports/cropan19.pdf

Van den Hoof, C., Hanert, E., & Vidale, P. L. (2011). Simulating dynamic crop growth with an adapted land surface model – JULES-SUCROS: Model development and validation. *Agricultural and Forest Meteorology*, *151*(2), 137–153. https://doi.org/10.1016/j.agrformet.2010.09.011

Vogel, M. M., Zscheischler, J., & Seneviratne, S. I. (2018). Varying soil moisture–atmosphere feedbacks explain divergent temperature extremes and precipitation projections in central Europe. *Earth System Dynamics*, *9*(3), 1107–1125. https://doi.org/10.5194/esd-9-1107-2018

Wakefield, R. A., Turner, D. D., & Basara, J. B. (2021). Evaluation of a land-atmosphere coupling metric computed from a ground-based infrared interferometer. *Journal of Hydrometeorology. Advance online publication*. https://doi.org/10.1175/JHM-D-20-0303.1

Warrach-Sagi. (2022). Selected data analysed in the JGR Atmosphere manuscript "Noah-MP with the generic crop growth model Gecros in the WRF model: Effects of dynamic crop growth on land-atmosphere interaction" [Data set]. Zenodo. https://doi.org/10.5281/zenodo.6501984

Warrach-Sagi, K., Mohr, V., & Wulfmeyer, V. (2018). High resolution WRF simulations for climate change studies in Germany. In W. E. Nagel, D. H. Kröner, & M. M. Resch (Eds.), *High performance computing in science and engineering ' 17* (pp. 431–440). Cham: Springer International Publishing. https://doi.org/10.1007/978-3-319-68394-2_25

Warrach-Sagi, K., Schwitalla, T., Wulfmeyer, V., & Bauer, H.-S. (2013). Evaluation of a climate simulation in Europe based on the WRF-NOAH model system: Precipitation in Germany. *Climate Dynamics*, *41*(3–4), 755–754. https://doi.org/10.1007/s00382-013-1727-7

Williams, I. N., & Torn, M. S. (2015). Vegetation controls on surface heat flux partitioning, and land-atmosphere coupling. *Geophysical Research Letters*, *42*(21), 9416–9424. https://doi.org/10.1002/2015GL066305

Wizemann, H.-D., Warrach-Sagi, K., Wulfmeyer, V., Ingwersen, J., Streck, T., & Högy, P. (2014). Three year observations of water vapor and energy fluxes over agricultural crops in two regional climates of Southwest Germany. *Meteorologische Zeitschrift*, *24*(1), 39–38. https://doi.org/10.1127/metz/2014/0618

Wulfmeyer, V., Branch, O., Warrach-Sagi, K., Bauer, H.-S., Schwitalla, T., & Becker, K. (2014). The impact of plantations on weather and climate in coastal desert regions. *Journal of Applied Meteorology and Climatology*, *53*(5), 1143–1142. https://doi.org/10.1175/JAMC-D-13-0208.1

Wulfmeyer, V., Späth, F., Behrendt, A., Jach, L., Warrach-Sagi, K., Ek, M. B., et al. (2020). The GEWEX land-atmosphere feedback observatory (GLAFO). Retrieved from https://www.gewex.org/gewex-content/files_mf/1583952472Feb2020.pdf

Wulfmeyer, V., Turner, D. D., Baker, B., Banta, R., Behrendt, A., Bonin, T. A., et al. (2018). A new research approach for observing and characterizing land–atmosphere feedback. *Bulletin of the American Meteorological Society*, *99*(8), 1639–1667. https://doi.org/10.1175/BAMS-D-17-0009.1

Yang, Z.-L., Niu, G.-Y., Mitchell, K., Chen, F., Ek, M. B., Barlage, M., et al. (2011). The community Noah land surface model with multiparameterization options (Noah-MP): 2. Evaluation over global river basins. *Journal of Geophysical Research*, *116*(D12), D12110. https://doi.org/10.1029/2010JD015140

Yin, X., & Schapendonk, A. (2004). Simulating the partitioning of biomass and nitrogen between roots and shoot in crop and grass plants. *NJAS - Wageningen Journal of Life Sciences*, *51*(4), 407–426. https://doi.org/10.1016/S1573-5214(04)80005-8

Yin, X., & van Laar, H. H. (2005). *Crop systems dynamics*. Wageningen Academic Publishers.

Zou, J., Xie, Z., Zhan, C., Chen, F., Qin, P., Hu, T., & Xie, J. (2019). Coupling of a regional climate model with a crop development model and evaluation of the coupled model across China. *Advances in Atmospheric Sciences*, *36*(5), 527–540. https://doi.org/10.1007/s00376-018-8160-0

Zscheischler, J., & Fischer, E. M. (2020). The record-breaking compound hot and dry 2018 growing season in Germany. *Weather and Climate Extremes*, *29*, 100270. https://doi.org/10.1016/j.wace.2020.100270